Colour and stellar population gradients in galaxies: correlation with mass

C. Tortora,[1,2]★ N. R. Napolitano,[3] V. F. Cardone,[4] M. Capaccioli,[2] Ph. Jetzer[1] and R. Molinaro[3,5]

[1]*Universität Zürich, Institut für Theoretische Physik, Winterthurerstrasse 190, CH-8057 Zürich, Switzerland*
[2]*Dipartimento di Scienze Fisiche, Università di Napoli Federico II, Compl. Univ. Monte S. Angelo, 80126 Napoli, Italy*
[3]*INAF – Osservatorio Astronomico di Capodimonte, Salita Moiariello, 16, 80131 Napoli, Italy*
[4]*Dipartimento di Fisica Generale A. Avogadro, Università di Torino and Istituto Nazionale di Fisica Nucleare - Sezione di Torino, Via Pietro Giuria 1, 10125 Torino, Italy*
[5]*Dipartimento di Fisica, Politecnico di Torino, Corso Duca degli Abruzzi 24, 10129 Torino, Italy*

ABSTRACT

We analyse the colour gradients (CGs) of ∼50 000 nearby Sloan Digital Sky Survey galaxies estimated by their photometrical parameters (Sérsic index, total magnitude and effective radius). From synthetic spectral models based on a simplified star formation recipe, we derive the mean spectral properties and explain the observed radial trends of the colour as gradients of the stellar population age and metallicity. CGs have been correlated with colour, luminosity, size, velocity dispersion and stellar mass. Distinct behaviours are found for early- and late-type galaxies (ETGs and LTGs), pointing to slightly different physical processes at work in different morphological types and at different mass scales.

In particular, the most massive ETGs ($M_* \gtrsim 10^{11}\,M_\odot$) have shallow (even flat) CGs in correspondence of shallow (negative) metallicity gradients. In the stellar mass range ($10^{10.3}-10^{10.5}$) $\lesssim M_* \lesssim 10^{11}\,M_\odot$, the metallicity gradients reach their minimum of $\sim -0.5\,\mathrm{dex}^{-1}$. At $M_* \sim 10^{10.3} - 10^{10.5}\,M_\odot$, colour and metallicity gradient slopes suddenly change. They turn out to anticorrelate with the mass, becoming highly positive at the very low masses, the transition from negative to positive occurring at $M_* \sim 10^{9-9.5}\,M_\odot$. These correlations are mirrored by similar trends of CGs with the effective radius and the velocity dispersion. We have also found that age gradients anticorrelate with metallicity gradients, as predicted by hierarchical cosmological simulations for ETGs. On the other side, LTGs have colour and metallicity gradients which systematically decrease with mass (and are always more negative than in ETGs), consistently with the expectation from gas infall and supernovae feedback scenarios.

Metallicity is found to be the main driver of the trend of CGs, especially for LTGs, but age gradients are not negligible and seem to play a significant role too. Owing to the large data set, we have been able to highlight that older galaxies have systematically shallower age and metallicity gradients than younger ones.

The emerging picture is qualitatively consistent with the predictions from hydrodynamical and chemodynamical simulations. In particular, our results for high-mass galaxies are in perfect agreement with predictions based on the merging scenario, while the evolution of LTGs and younger and less massive ETGs seems to be mainly driven by infall and supernovae feedback.

Key words: galaxies: elliptical and lenticular, cD – galaxies: evolution – galaxies: general – dark matter.

1 INTRODUCTION

Galaxy formation is a complicated matter which has not yet come to a complete and coherent understanding. The standard cosmological paradigm, the so-called Λ cold dark matter (CDM), predicts that dark matter (DM) haloes evolve hierarchically since early epochs,

★E-mail: ctortora@na.astro.it

with smaller units merging into massive structures (Kauffmann & White 1993; de Lucia et al. 2006; Ruszkowski & Springel 2009), which find positive evidences in the strong size evolution in massive galaxies since $z \sim 3$ (Glazebrook et al. 2004; Daddi et al. 2005; Trujillo et al. 2006). This scenario is at variance with the evidences that today's high mass galaxies formed most of their stars in earlier epochs and over a shorter time interval than low-mass ones. This 'downsizing' scheme (Cowie et al. 1996; Gallazzi et al. 2005; Jimenez et al. 2005; Nelan et al. 2005; Thomas et al. 2005; Treu et al. 2005; Bundy et al. 2006; Cimatti, Daddi & Renzini 2006; Pannella et al. 2006; Panter et al. 2007; Fontanot et al. 2009) seems at odd with the ΛCDM hierarchical growth and seems rather to support a 'monolithic-like' formation scheme (see e.g. Chiosi & Carraro 2002) which broadly predicts an inside-out formation of stars after an early dissipative collapse.

However, it is increasingly clearer that the downsizing is compatible with the hierarchical model if the feedback processes in the mass accretion history of the ΛCDM dark haloes are taken into account (see e.g. Neistein, van den Bosch & Dekel 2006; Cattaneo et al. 2008; Conroy & Wechsler 2009; Cattaneo et al. 2010). On the one hand, the gas cooling and the shock heating (Dekel & Birnboim 2006; Cattaneo et al. 2008) are the main drivers of the star formation (SF) activity during the hierarchical growth of the DM haloes; on the other side, supernovae (SNe), active galactic nuclei (AGN), merging, harassment, strangulation etc., generally inhibit the stellar formation (Dekel & Silk 1986; Recchi, Matteucci & D'Ercole 2001; Pipino et al. 2002; di Matteo, Springel & Hernquist 2005; Cattaneo et al. 2006; de Lucia et al. 2006; Scannapieco et al. 2006; Kaviraj et al. 2007; Schawinski et al. 2007; Antonuccio-Delogu & Silk 2008; Cattaneo et al. 2008; Khalatyan et al. 2008; Romeo et al. 2008; Tortora et al. 2009b; Weinmann et al. 2009).

The different processes might rule the SF at the global galaxy scale, or act at subgalactic scales (e.g. the nuclear regions versus outskirts) such that they are expected to introduce a gradient of the main stellar properties with the radius that shall leave observational signatures in galaxy colours.

This paper is motivated by the fact that colour gradients (CGs) are efficient markers of the stellar properties variations within galaxies, in particular as they mirror the gradients of star ages and metallicities (Sandage 1972), although it is not yet fully clear whether metallicity is the main driver of the CGs in normal spheroidal (Saglia et al. 2000; Tamura & Ohta 2000; La Barbera et al. 2002, 2003; Kobayashi 2004; Spolaor et al. 2009; Rawle, Smith & Lucey 2010) and late-type systems (MacArthur et al. 2004; Taylor et al. 2005), or age plays also an significant role (Saglia et al. 2000; La Barbera et al. 2003; MacArthur et al. 2004; Spolaor et al. 2009; Rawle et al. 2010).

CGs are primarily a tool to discriminate the two broad formation scenarios (monolithic versus hierarchical), but more importantly they provide a deeper insight on the different mechanisms ruling the galaxy evolution. As these mechanisms depend on the galaxy mass scale, the widest mass (and luminosity) observational baseline is needed to remark the relative effectiveness of the different physical processes and their correlation with the observed population gradients.

The observational picture is so complex to justify a schematic review of the evidences accumulated so far. The facts are as follows.

(1) On average, nearby elliptical and spiral galaxies are bluer outwards (Franx, Illingworth & Heckman 1989; Peletier et al. 1990a; Peletier, Valentijn & Jameson 1990b; Balcells & Peletier 1994; Tamura & Ohta 2003), while dwarfs show mainly redder outskirts (Vader et al. 1988; Kormendy & Djorgovski 1989; Chaboyer 1994;

Tully et al. 1996; Jansen et al. 2000; Scodeggio 2001; Cameron et al. 2009). Recently, deeper investigations of later type galaxies have been done and have highlighted the presence of non-monotonic colour and stellar population gradients in these systems (MacArthur et al. 2004; Bakos, Trujillo & Pohlen 2008; MacArthur, González & Courteau 2009; Martínez-Serrano et al. 2009; Sánchez-Blázquez et al. 2009).

(2) Spectral line indices (mainly measured in early-type galaxies, ETGs) are somehow a more efficient tracer of the stellar population properties and generally found to change with the radius like CGs (Kobayashi & Arimoto 1999; Kuntschner et al. 2006; MacArthur et al. 2009; Rawle et al. 2010).

(3) Interpreting CGs in terms of metallicity gradients, in high-mass galaxies typically $d \log Z/d \log R \sim -0.3$, which is shallower than predicted by simulations of dissipative 'monolithic' collapse (where -0.5 or a steeper value is expected, see e.g. Larson 1974, 1975; Carlberg 1984; Arimoto & Yoshii 1987; Kobayashi 2004, see also below).

(4) There are contradictory evidences of a correlation of CGs with galaxy mass and luminosity. Earlier studies have claimed a weak correlation with the physical properties of galaxies (e.g. mass, luminosity, etc., Peletier et al. 1990a; Davies, Sadler & Peletier 1993; Kobayashi & Arimoto 1999; Tamura & Ohta 2003), at variance with the typical monolithic collapse predictions. Recently, a stronger correlation with mass has started to emerge (e.g. Forbes, Sánchez-Blázquez & Proctor 2005), pointing to a metallicity gradient decreasing with the mass for low-mass galaxies (Spolaor et al. 2009; Rawle et al. 2010), accordingly with the monolithic scenario. Instead, high-mass galaxies show too shallow gradients to match the predictions of the monolithic collapse, but compatible with galaxy merging.

This wealth of observational evidences must be confronted with the model predictions coming from the different galaxy formation scenarios.

(1) Steep gradients are expected when stars form during strong dissipative (monolithic) collapses in deep potential wells of galaxy cores where the gas is more efficiently retained, with a consequent longer SF activity and a longer chemical enrichment in the inner than in outer regions (negative metallicity gradients). On top of that, the delayed onset of winds from SNe, causing a further metal supply in the central regions, would contribute to reinforce the steepness of these gradients (see, e.g. Pipino, D'Ercole & Matteucci 2008). As these processes are regulated by the galaxy potential depth, which is somehow related to the galaxy mass (and luminosity),[1] high-mass galaxies are expected to have metallicity gradients which are steeper than lower-mass ones. The latter seem to have almost no gradients (Gibson 1997; Chiosi & Carraro 2002; Kawata & Gibson 2003), although the results here are based on limited galaxy samples.

(2) Within the hierarchical picture, merging induces a meshing of stellar populations, and lead to a more uniform metallicity distribution and to shallower CGs (White 1980; Kobayashi 2004). Strong jets from powerful AGNs can also quench the SF on the global galaxy scale and flatten colours gradients in the host systems (Tortora et al. 2009b).

---

[1]It remains to be seen whether there might be a correlation with the DM fraction of the systems which is also a function of the galaxy stellar mass (see e.g. Napolitano et al. 2005; Cappellari et al. 2006; Conroy & Wechsler 2009; Tortora et al. 2009a; Napolitano, Romanowsky & Tortora 2010).

(3) Metallicity and CGs seem also to depend on the efficiency of the dissipative processes in dark haloes (Hopkins et al. 2009a), with just a weak dependence on the remnant mass (Bekki & Shioya 1999; Kobayashi 2004; Hopkins et al. 2008b), in a way more similar of the observed gradients. However, while merging is crucial to smear out the colour radial variation in high-mass galaxies (Kobayashi 2004), it seems unimportant for low-mass systems (de Lucia et al. 2006; Cattaneo et al. 2008). Instead, the energy from stellar winds and SNe and the effect of dissipative collapse might induce even positive steep gradients (Mori et al. 1997).

CGs are the most direct observables to investigate the effect of the physical processes (such as merging, AGN, SNe, stellar feedback), which drive the galaxy evolution as a function of the main galaxy parameters: luminosity, mass and central velocity dispersion. In this paper, we analyse optical CGs in about 50 000 Sloan Digital Sky Survey (SDSS) local galaxies, spanning a wide range of luminosities and masses. CGs are obtained in an indirect way from the photometrical parameters of the individual galaxies (effective radius, Sérsic index, total magnitude). Using synthetic spectral models, we compute age and metallicity gradients for early- and late-type systems and analyse the trends with mass. The sample allows us to investigate the distribution of the CGs over an unprecedented baseline of galaxy sizes, luminosities, velocity dispersions and stellar masses. The observed trends are interpreted by means of quite different physical phenomena at the various mass scales. This approach, while exposed to the uncertainties on the structural parameters (e.g. Sérsic index, n, and effective radius, R_{eff}), has the advantage of dealing with large statistics; furthermore it is exportable to higher redshift galaxy surveys which are generally limited to rest-frame visual bands. In this respect, we pay particular care in checking the consistency of our results with independent analyses. We will mainly concentrate on ETGs, for which a wide collection of results (having an homogenized gradient definition) is available from literature. On the other hand, due to the uncertainties of the structural parameters of late-type galaxies (LTGs), we will take the results on this galaxy sample with the right caution, being well aware that our findings might be only a benchmark for more accurate analyses.

In Section 2 we present the data sample and spectral models. In Section 3 we show the main results of our analysis, discussing CGs as a function of structural parameters, stellar masses and stellar properties derived from the fitting procedure. In the same section, age and metallicity gradients are shown, and discussed within the galaxy formation scenarios in Section 4. We finally draw some conclusions in Section 5.

In the following, we use a cosmological model with $(\Omega_m, \Omega_\Lambda, h) = (0.3, 0.7, 0.7)$, where $h = H_0/100\,km\,s^{-1}\,Mpc^{-1}$ (Spergel et al. 2003, 2007), corresponding to a Universe age of $t_{univ} = 13.5\,Gyr$.

2 DATA

2.1 Galaxy sample

Our data base consist of 50 000 low-redshift ($0.0033 \leq z \leq 0.05$) galaxies in the New York University Value-Added Galaxy Catalogue (NYU-VAGC) extracted from SDSS DR4 (Blanton et al. 2005b, hereafter B05).[2] B05 have performed a set of quality checks

contemplating the analysis of large and complex galaxies, incorrectly deblended in the SDSS pipeline, and of the star/galaxy separation, with a number of eyeball inspections on objects in the catalogue. The catalogue includes Petrosian magnitudes and structural parameters in *ugriz* bands such as the concentrations $C = R_{90}/R_{50}$, where R_{90} and R_{50} are the Petrosian radii enclosing 90 and 50 per cent of total luminosity. Effective radius, R_{eff}, and the Sérsic indices n are taken from B05, where a 1D seeing-convolved Sérsic profile is fitted to galaxies. The adopted redshift range sets the completeness level at a Petrosian magnitude $r \simeq 18$ and at a surface brightness within R_{50} $\mu_{50} \simeq 24.5\,mag\,arcsec^{-2}$. This luminosity limited sample still suffers from an incompleteness at low surface brightness levels, e.g. in the regime of dwarf galaxies with $M_* \lesssim 10^{8.3} - 10^{8.5}\,M_\odot$ (Blanton et al. 2005a; Baldry, Glazebrook & Driver 2008; Li & White 2009). Moreover, the incompleteness, almost negligible for more massive galaxies, comes back again for the most massive ones ($M_* \gtrsim 10^{11}\,M_\odot$) as the sample is biased against large objects at lower redshifts in consequence of a bias in the SDSS photometric pipeline (Blanton et al. 2005a). We address the systematics of the SDSS sample more in detail in Appendix A1.

Petrosian magnitudes are reduced to $z = 0$ (K term; Blanton et al. 2003a), corrected for galactic extinction using the Schlegel, Finkbeiner & Davis (1998) dust map, converted to our adopted cosmology (Blanton et al. 2003b), and further corrected for the missing flux of Petrosian magnitudes. The latter correction is almost unchanged using the relation in Graham et al. (2005).

The sample spans a wide range of luminosities, masses and colours, including galaxies lying both in the red sequence (RS) and in the blue cloud (BC). In particular, we have sorted out ETGs by adopting the following two criteria:

(i) the r-band Sérsic index satisfies the condition $2.5 \leq n \leq 5.5$;
(ii) the r-band concentration index $C > 2.6$ (Shimasaku et al. 2001; Padmanabhan et al. 2004; Capozziello et al. 2007).[3]

The final ETG sample consists of 10 508 galaxies. Of the remaining entries of our data base, 27 813 are LTGs, defined as objects with $C \leq 2.6$, $n \leq 2.5$ and $\sigma_0 \leq 150\,km\,s^{-1}$, and 9 359 are intermediate morphology galaxies, with $C \leq 2.6 (>2.6)$ and $n > 2.5 (\leq 2.5)$, hereafter named intermediate-type galaxies (ITGs).[4] Further details on the adopted morphology criteria are given in the Appendix A2. In this paper, we will consider ETGs and LTGs only, with a main focus on ETGs.

2.2 Spectral models and gradients

The stellar population analysis of the selected sample is based on a set of 'single burst' synthetic stellar spectra using the prescription of Bruzual & Charlot (2003, hereafter BC03). These models are widely used in literature both for ellipticals and spirals (e.g. Trager et al. 2000; Bell & de Jong 2001; Ganda et al. 2007; Peletier et al. 2007), but we are aware that, in some cases, e.g. in later-type systems with very protracted SFs (Kennicutt 1983), they may fail to reproduce correctly the galaxy properties (MacArthur et al. 2009). A finer analysis would require a more realistic SF history for LTGs (e.g. an

---

[2] The catalogue is available at: http://sdss.physics.nyu.edu/vagc/lowz.html.

[3] In order to retain the low-mass red systems, no lower cut has been applied to the velocity dispersion. However, very low values ($\sigma_0 < 70\,km\,s^{-1}$) may be prone to large systematics, due to the signal-to-noise ratio and instrumental resolution of the SDSS spectra.

[4] Note that 2120 galaxies are cut away by the conservative upper limit on n, dictated by the fitting Sérsic code limit of $n = 6$.

exponentially decaying or a constant SF), which is beyond the scope of this paper.

We adopt a Chabrier (2001, 2002, 2003) initial mass function (IMF), noting that the choice of a Salpeter (1955) IMF would affect the total stellar mass only, shifting $\log M_*$ upward by ~ 0.25 and leaving all the other stellar population parameters unchanged (e.g. Tortora et al. 2009a). Our choice of the BC03 models is driven by their high versatility and ability to span the stellar parameter space, e.g. metallicities and ages. There are other options (Rettura et al. 2006; Kannappan & Gawiser 2007; Tortora et al. 2009a, for a comparison of the results from different prescriptions), but none is found to be bias free (Maraston 2005; van der Wel et al. 2006; Conroy, Gunn & White 2009, 2010; Maraston et al. 2009; Conroy & Gunn 2010).

In our model procedures we adopt a metallicity ranging within 0.0001–0.05, and the Universe age, t_{univ} (in the assumed cosmology), as an upper limit for the galaxy ages. Synthetic colours have been obtained after convolving the spectra with the corresponding SDSS filter bandpass functions. To improve the sensitivity of the results to the small differences in both Z and ages, we have adopted a 'mesh refinement' procedure which interpolates the synthetic models over the initial grid of equally spaced bins in the logarithm of Z and age. To estimate the galaxy age, Z, and the stellar mass-to-light ratio, Υ_*, we use a χ^2 minimization fit (see Tortora et al. 2009a,b for details) to the observed colours ($u - g$, $g - r$, $g - i$ and $g - z$). It is known that the use of just the optical broad-bands is severely prone to the well-known age–metallicity degeneracy. However, following previous indications (e.g. Wu et al. 2005) we have verified in Appendix B that the use of near infrared (NIR) photometry reduces the overall uncertainties but does not modify the estimates of the intrinsic population parameters based on optical bands only. We shall return on this issue later on.

We have used the structural parameters given by B05 to derive the colour profile $(X - Y)(R)$ of each galaxy as the differences between the (logarithmic) surface brightness measurements in the two bands, X and Y. The CG is defined as the angular coefficient of the relation $X - Y$ versus $\log R/R_{eff}$, $\nabla_{X-Y} = \delta(X - Y)/\delta \log(R/R_{eff})$, measured in mag dex^{-1} (omitted in the following unless needed for clarity). The fit of each colour profile is performed in the range $R_1 = 0.1 R_{eff} \leq R \leq R_2 = R_{eff}$. We have verified that a choice of different radial ranges for the fit leaves the global trends unaffected. In particular, by setting $R_2 = 2 R_{eff}$ the gradients changed by $\lesssim 0.01 - 0.02$ mag, where R_{eff} is the r-band effective radius (Peletier et al. 1990b; La Barbera et al. 2005). Slightly different definitions are also used elsewhere (see discussion in Liu et al. 2009).

By definition, a positive CG, $\nabla_{X-Y} > 0$, means that a galaxy is redder as R increases, while it is bluer outward for a negative gradient. The fit of synthetic colours is performed on the colours at R_1 and R_2 and on the total integrated colours. Following La Barbera et al. (2005) we define the stellar parameters gradients as $\nabla_{age} = \log[age_2/age_1]$ and $\nabla_Z = \log[Z_2/Z_1]$, where (age$_i$, Z_i) with $i = 1, 2$ are the estimated age and metallicity at R_1 and R_2, respectively.

A full test of the reliability of our modelling technique, the presence of spuriously generated correlations and the contribution from internal dust extinction are addressed in Appendix B.

3 RESULTS

We show how colour and stellar population gradients depend on structural parameters and mass, and compare the results with the predictions from galaxy formation scenarios. The median trends,

e.g. in bins of mass, velocity dispersion, colours etc., will be represented along with the 25th–75th percentiles in each bin.

The average behaviour of galaxies is analysed in the parameter space, and the galaxy properties discussed after splitting the sample in the two morphological classes, ETGs and LTGs. We concentrate mainly on the analysis of ETGs and compare our findings with a wide collection of independent data and simulations.

3.1 CGs as a function of structural parameters, luminosity and mass

Fig. 1 presents the gradients ∇_{g-i} as a function of integrated colours, structural parameters, r-band magnitude, central velocity dispersion and stellar mass. We adopted the $g - i$ colour as a reference having verified that the use of different colours does not affect our conclusions. As shown in the top-left panel of the figure, CGs are, on average, positive for the galaxies with bluer colours, $g - i \lesssim 0.5$, while they reach increasingly negative values for redder galaxies (e.g. Park & Choi 2005; Lee et al. 2007; Suh et al. 2010). Since $g - i \sim 0.5$ marks the transition from the RS to the BC, this result allows us to broadly associate negative and positive CGs to the RS and BC, respectively. Furthermore, galaxies with intermediate colours ($g - i \sim 0.5$–0.7 or equivalently $g - r \sim 0.2$–0.6) have almost null (or slightly negative) gradients. The same trend holds by considering central and outer colours (at $R = R_1$ and R_2). We will return to this issue later on.

Tight trends are found when plotting the gradients against the r-band total magnitude and stellar mass, while the dependence on σ_0 is weaker. In the latter case, gradients look negative almost everywhere with the less massive galaxies ($\log \sigma_0 < 2 \, \text{km s}^{-1}$) having the smallest $\nabla_{g-i} (\sim -0.2)$. Although our sample does not include very massive galaxies ($M_* \gtrsim 10^{11.5} \, \text{M}_\odot$), our results seem to show a stable trend at the large mass scales, pointing to even shallower gradients. We note here that the smaller range shown by ∇_{g-i} as a function of σ_0 in the central panel (left column) of Fig. 1 is mainly due to the mix of the ETGs and LTGs. They have different trends with small σ_0 in the low mass regime (see also Section 3.2), thus producing a dilution of the average gradients with respect, e.g. the larger median $\nabla_{g-i} (\sim 0 \div 0.2)$ found for the low stellar mass (right column).

The correlations with luminosity and mass show that, starting from the bright/massive end, the CGs become steeper, with the steepest negative gradients (~ -0.2) corresponding to $r \sim -20$ mag and $M_* \sim 10^{10.3} \, \text{M}_\odot$. From there, bluer and later type systems begin to dominate, and the gradients invert the trend with luminosity and mass, becoming positive at $r \sim -17.5$ mag and $M_* \sim 10^{8.7} \, \text{M}_\odot$. The lowest mass systems are those with the highest, positive gradients (~ 0.2). The mass scale at which the CG trend inverts is in remarkable agreement with the typical mass scale break for 'bright' and 'ordinary' galaxies (Capaccioli, Caon & D'Onofrio 1992a, see also Section 3.2) or for star-forming and passive systems (Kauffmann et al. 2003; Drory & Alvarez 2008).

The above trend holds also for the correlation with R_{eff} and, less strongly, with the Sérsic index, n, as expected in view of the tight correlation with stellar mass and luminosity (Caon, Capaccioli & D'Onofrio 1993; Prugniel & Simien 1997; Graham & Guzmán 2003; Shen et al. 2003; Trujillo et al. 2004a; Tortora et al. 2009a). Note that the minimum at $n \sim 2$ for the trend of the gradient (Fig. 1, bottom right) roughly coincides with the value used here to set the separation between ETG and LTG systems, suggesting differences in the CG properties.
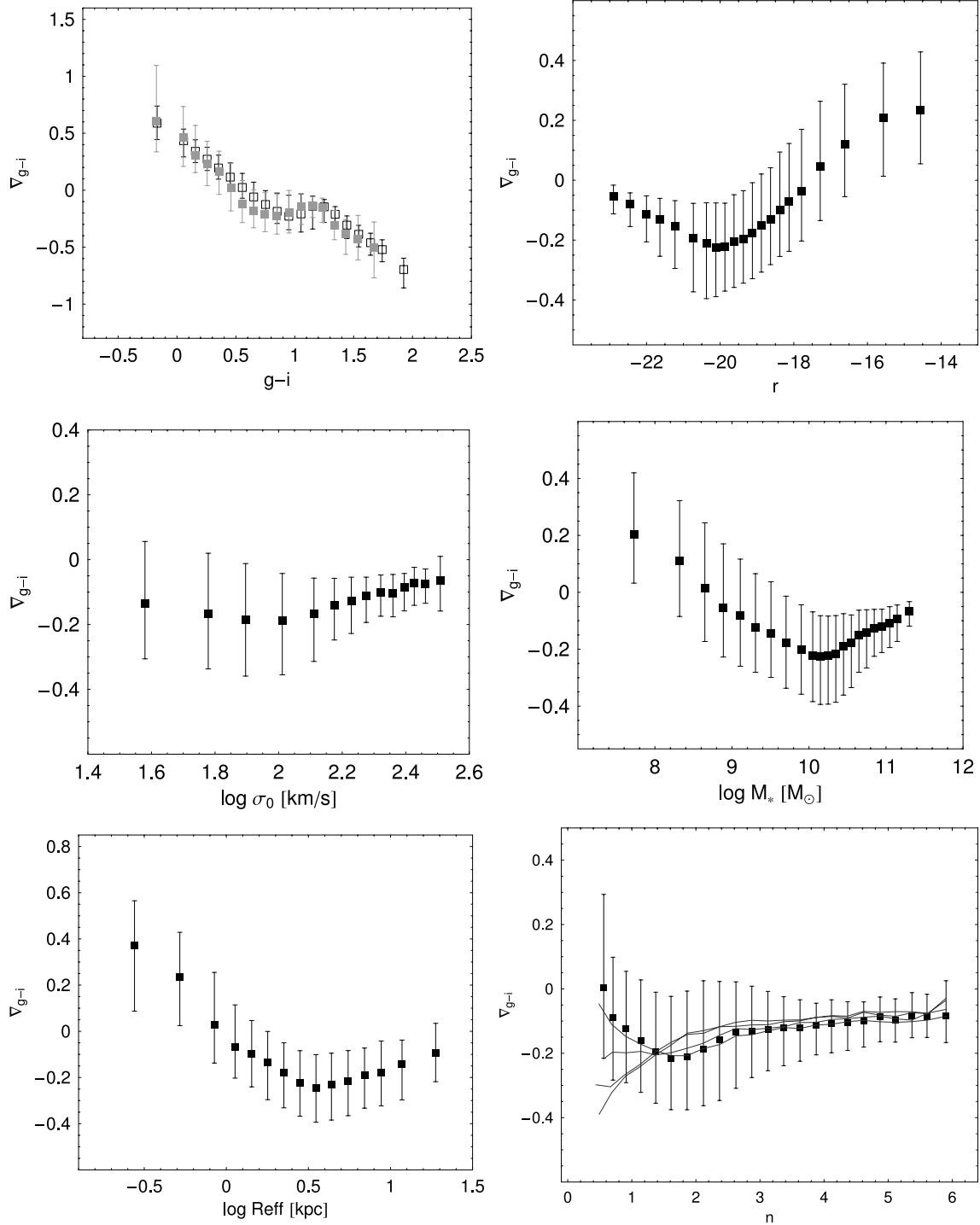
Figure 1. Gradients of the $g-i$ colour, as a function of various observed and derived quantities. Medians of binned CGs are plotted together with the 25–75 per cent quantiles, shown as error bars. Top left: CG as a function of colour, black open and grey squares are for colours at R_1 and R_2, respectively. Top right: CG as a function of r-band magnitude. Middle left: CG as a function of logarithm of σ_0, which is defined as the velocity dispersion within a circular aperture of radius $0.1R_{\rm eff}$ (using r-band $R_{\rm eff}$) from the SDSS velocity dispersion $\sigma_{\rm ap}$, using the relation in Jørgensen, Franx & Kjærgaard (1995, 1996). Middle right: gradient as a function of total stellar mass M_* (assuming a Chabrier IMF), which is the output of our stellar population analysis fitting the total colours. Bottom left: CG as a function of logarithmic of r-band $R_{\rm eff}$ (the results do not depend on the band). Bottom right: CG as a function of i-band Sérsic index n; the lines are the median trends for the Sérsic index in the other bands.

3.2 Gradients in morphologically selected galaxies

Following the dependence of ∇_{g-i} versus n just discussed, ETG and LTG samples will be now considered separately. In Fig. 2 we plot ∇_{g-i} versus $R_{\rm eff}$, σ_0, and M_* for ETGs (red symbols) and LTGs (blue symbols). The slopes of the linear best-fitting relations of the CGs versus σ_0 and M_* are shown in Table 1.
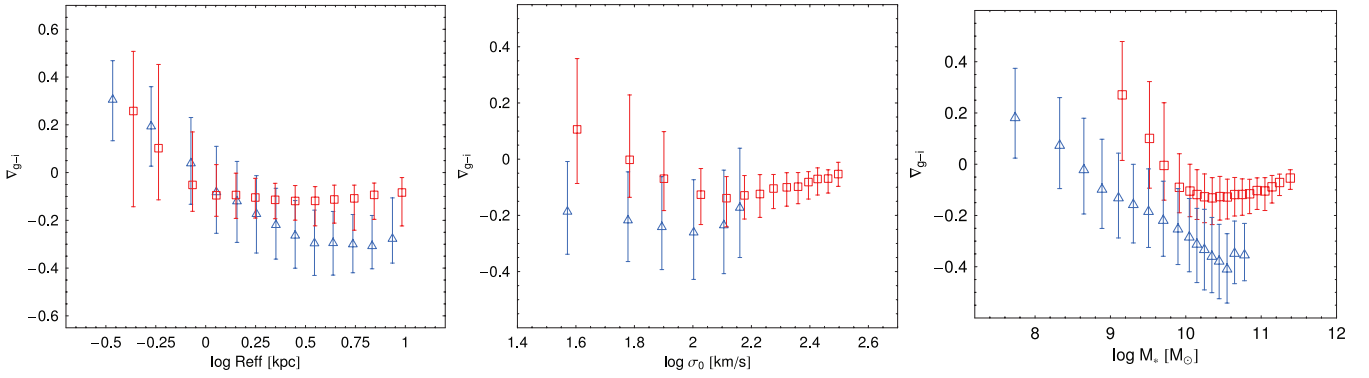
Figure 2. ∇_{g-i} as a function of effective radius (left-hand panel), velocity dispersion (middle panel) and stellar mass (right-hand panel) for ETGs (open red boxes) and LTGs (open blue triangle).

Table 1. Slopes of the correlation between CGs (∇_{u-g}, ∇_{g-r}, ∇_{g-i}, ∇_{g-z}), ∇_{age} and ∇_Z versus $\log \sigma_0$ and $\log M_*$ for ETGs and LTGs. The errors on slopes are computed as 1σ uncertainty by a bootstrap method.

Correlation	γ_{ETG}		γ_{LTG}
	$\log \sigma_0 < 2.2$	$\log \sigma_0 > 2.2$	
∇_{u-g}–$\log \sigma_0$	-0.60 ± 0.03	0.40 ± 0.05	0.02 ± 0.05
∇_{g-r}–$\log \sigma_0$	-0.27 ± 0.01	0.19 ± 0.01	-0.02 ± 0.02
∇_{g-i}–$\log \sigma_0$	-0.34 ± 0.02	0.25 ± 0.04	-0.03 ± 0.02
∇_{g-z}–$\log \sigma_0$	-0.40 ± 0.02	0.17 ± 0.04	-0.09 ± 0.03
∇_{age}–$\log \sigma_0$	-0.10 ± 0.03	0.04 ± 0.17	0.14 ± 0.02
∇_Z–$\log \sigma_0$	-0.86 ± 0.07	1.02 ± 0.24	0.06 ± 0.10
	$\log M_* < 10.3$	$\log M_* > 10.3$	
∇_{u-g}–$\log M_*$	-0.43 ± 0.04	0.12 ± 0.02	-0.30 ± 0.01
∇_{g-r}–$\log M_*$	-0.24 ± 0.02	0.05 ± 0.01	-0.13 ± 0.01
∇_{g-i}–$\log M_*$	-0.34 ± 0.02	0.07 ± 0.01	-0.18 ± 0.01
∇_{g-z}–$\log M_*$	-0.36 ± 0.03	0.02 ± 0.01	-0.18 ± 0.01
∇_{age}–$\log M_*^\star$	-0.18 ± 0.06	0.24 ± 0.03	-0.01 ± 0.01
∇_Z–$\log M_*$	-0.46 ± 0.06	0.10 ± 0.04	-0.45 ± 0.01

*For the LTG sample, splitting galaxies by masses smaller/larger than $\log M_* \sim 10.3$ would result in slopes of -0.07 ± 0.01 and 0.26 ± 0.25, respectively.

Figure 3. CG ∇_{g-r} as a function of r-band magnitude for ETG sample. Superimposed are the results from La Barbera et al. (2005) for high-richness (open boxes), low-richness (filled boxes) and all (crosses) the clusters. The blue and red arrows are the median ∇_{g-r} for the massive galaxies analysed in Wu et al. (2005) and La Barbera & de Carvalho (2009) respectively; see the text for details.

First, ETGs are on average brighter and more massive than LTGs (Kauffmann et al. 2003) and have less dispersed CGs. As a general result, large R_{eff} galaxies are found to have lower gradients than more compact systems (e.g. Hopkins et al. 2009a). However, for LTGs, ∇_{g-i} monotonically decreases with R_{eff} and becomes flat at $\log R_{eff} \gtrsim 0.5$, while for ETG it slightly increases for $\log R_{eff} \gtrsim 0.3$, and decreases for smaller R_{eff}. Similar trends are observed for the gradients as a function of the stellar mass. LTGs show a monotonic decreasing trend (in qualitative agreement with Kim & Ann 1990 and Liu et al. 2009), while a U-shaped function is found for ETGs with the gradients definitely decreasing with the mass for $M_* \lesssim 10^{10.3}$–$10^{10.5}$ $M_\odot$, and a mildly increasing for larger mass values. This mass scale roughly corresponds to a total luminosity of $r \sim -20.5$ mag, which is compatible with the typical luminosity (and mass) scale for ETG dichotomy in the galaxy structural properties (e.g. Bender et al. 1989; Capaccioli et al. 1992a; Capaccioli, Caon & D'Onofrio 1992b; Graham & Guzmán 2003; Graham et al. 2003; Trujillo et al. 2004b; Kormendy et al. 2009). As discussed in Capaccioli et al. (1992a), this dichotomy may be related to the formation mechanism processes, and in particular to the dominance of the merging events for the 'bright' sample, which is compatible with the shallower gradients that we observe for these systems
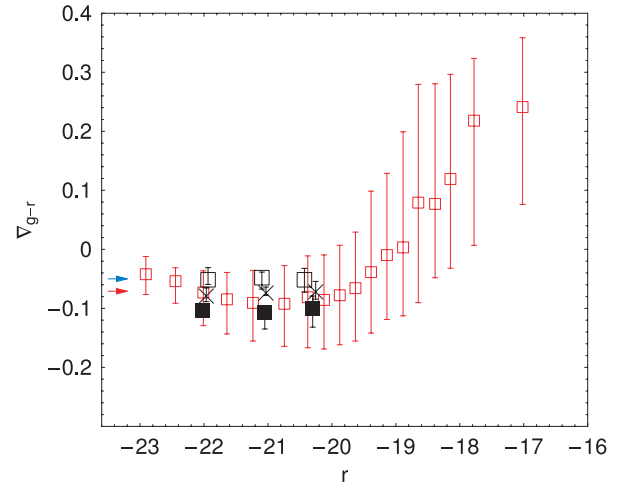
(see, e.g. Fig. 2, right-hand panel). Nevertheless, for a fixed stellar mass we observe that ETGs gradients are, on average, larger than LTG ones. The same two-fold trend is shown for ETGs gradients as function of the velocity dispersion, while no trend is observed for LTGs gradients.

As a consistency check, in Fig. 3 we superpose to our $g-r$ gradients as a function of the r-band luminosity the results of La Barbera et al. (2005) obtained by analysing a sample of low-redshift luminous ($r \le -20$ mag) cluster galaxies. Their value ($\nabla_{g-r} \sim -0.075$) is in agreement with our findings over the range where the two studies overlap, but we were also able to identify a change of ∇_{g-r} with our larger luminosity baseline. The results from the massive galaxies in Wu et al. (2005) and La Barbera & de Carvalho (2009) are also shown to have ∇_{g-r} consistent with our results.

Unfortunately, we have no information on the environment of the individual systems in our sample, to check the dependence of our results with the local density. There are many lines of evidences that ETGs in clusters (and in very dense environments in general) have shallower gradients than systems in less dense environments (Tamura & Ohta 2000; Tamura et al. 2000; La Barbera et al. 2005, see also Fig. 3). However, according to the morphological segregation, LTGs, which are expected to reside in the field or in
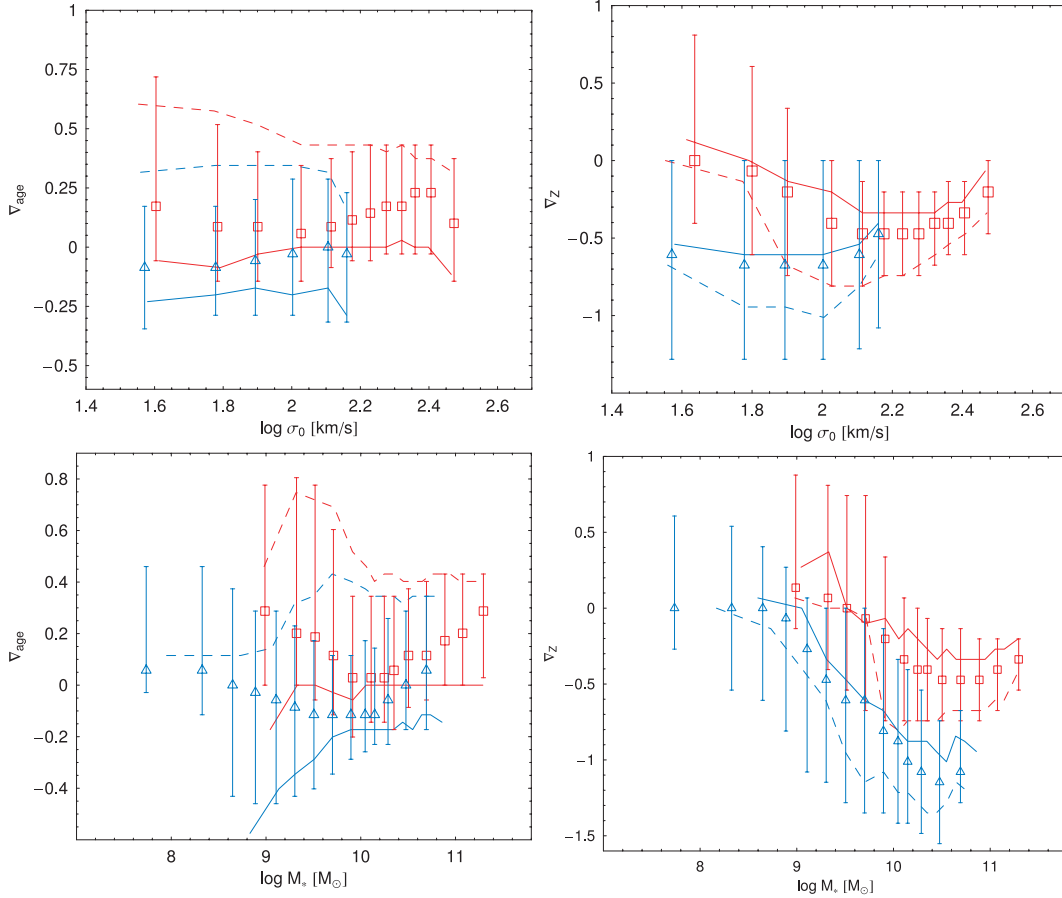
Figure 4. Age and metallicity gradients as a function of velocity dispersion (top panels) and stellar mass (bottom panels). Solid and dashed lines are for galaxies with central stellar populations older and younger than 6 Gyr, respectively. Symbols are as in Fig. 2

the external regions of clusters, have indeed lower gradients than ETGs which are found to live mainly in higher density environments.

3.3 Interpretation in terms of Z and age gradients

Here we test whether the CGs can be explained in terms of stellar properties such as age and metallicity. As seen in Section 2, we have obtained the gradients of metallicity and age distributions using two characteristic scales ($0.1 R_{\rm eff}$ and $1 R_{\rm eff}$). The $\nabla_{\rm age}$ and ∇_Z are shown in Fig. 4 as a function of the velocity dispersion and the stellar mass, and the fitted slopes of such relations are quoted in Table 1.

Some features survive the large scatter. For LTGs the $\nabla_{\rm age}$ is about zero both with σ_0 and mass, strongly suggesting that CGs should not depend on age gradients of the galaxy stellar population.[5] Actually, ∇_Z is instead strongly dependent on M_*, with the lowest metallicity gradients (~ -1) at the largest masses, while the dependence on σ_0 is very weak as the $\nabla_Z \sim (-0.5, -0.6)$ for all σ_0.

ETG age gradients seem basically featureless when plotted against σ_0, where we find $\nabla_{\rm age} > 0$ with typical median values of $\nabla_{\rm age} \sim 0.2$. On the other hand, the metallicity gradients show some features with ∇_Z decreasing for $\log \sigma_0 \lesssim 2.2 \,{\rm km\,s}^{-1}$,

with a slope $= -0.86$, and increasing for larger velocity dispersion, with a slope of 1.02, reaching the shallowest values (~ -0.2) at $\log \sigma_0 \gtrsim 2.4 \,{\rm km\,s}^{-1}$ and at the very low σ_0 (i.e. $\log \sigma_0 < 1.8 \,{\rm km\,s}^{-1}$) where $\nabla_Z \sim 0$. This peculiar trend is mirrored by a similar dependence on the stellar mass.[6] This two-fold behaviour is also significant when we plot $\nabla_{\rm age}$ as a function of the stellar mass: $\nabla_{\rm age}$ decreases at $\log M_* \lesssim 10.3\text{--}10.5$, and increases in more massive systems.

Bright ETGs with $r \lesssim -20$ mag ($\log M_* \gtrsim 10$) have a median $\nabla_{\rm age} = 0.144^{+0.004}_{-0.003}$ (with scatter $^{+0.26}_{-0.17}$) and $\nabla_Z = -0.472^{+0.005}_{-0.004}$ (with scatter $^{+0.34}_{-0.27}$), where the error bars represent the 1σ uncertainty and the scatters the 25–75 percentiles of the sample distribution. However, we have found that $\nabla_{\rm age}$ and ∇_Z strongly depend on galaxy age: in particular, if we separate the sample in systems with older and younger than 6 Gyr central stars, we obtain different age and metallicity gradient trends as shown in Fig. 4. Older systems have gradients which are shallower than younger (in particular for ETGs) and bracket the average trend of the whole samples. A partial

[5] The scatter of the gradients around zero has been suggested to be a manifestation of possible differences in the formation processes in these systems MacArthur et al. (2009).

[6] For ETGs, stellar mass and σ_0 are tightly correlated, thus the correlation and the interpretation discussed here can be made when dissecting the similar trend as a function of velocity dispersion. On the contrary, many low-mass LTGs have very large velocity dispersion which contribute to have almost constant metallicity gradients for $\log \sigma_0 \lesssim 2.2 \,{\rm km\,s}^{-1}$ and increasing at larger σ_0. But in this case the scatter is very large suggesting that the central velocity dispersion is not a representative parameter of such rotational velocity supported systems.

contribution to the scatter is also given by the central metallicity: the lower Z systems show generally shallower gradients and vice versa. However, the effect is significantly smaller with respect to the central age.

The median values of the older sample is $\nabla_{\rm age} = 0^{+0.003}_{-0.004}$ (with scatter $^{+0.14}_{-0.14}$) and $\nabla_Z = -0.337^{+0.006}_{-0.005}$ (with scatter $^{+0.27}_{-0.20}$) while for the younger one, we obtain $\nabla_{\rm age} = 0.43^{+0.001}_{-0.006}$ (with scatter $^{+0.08}_{-0.20}$) and $\nabla_Z = -0.67^{+0.007}_{-0.004}$ (with scatter $^{+0.27}_{-0.13}$). Galaxies with old central ages are fully consistent with the results of pure metallicity and mixed age+metallicity models in La Barbera et al. (2005) and with the best-fitted values in La Barbera & de Carvalho (2009) (where galaxy ages are in the range of 7.8–12.6 Gyr). The agreement with Rawle et al. (2010) is also good if we consider that their sample has a median central age of $\sim$10 Gyr (calculated within an $R_{\rm eff}/3$ aperture), comparable to the old objects of our sample: they find an age gradient of -0.02 ± 0.06 and metallicity gradients of -0.13 ± 0.04. Finally, from the analysis of 36 nearby ETGs with SDSS and Two-Micron All-Sky Survey (2MASS) photometry, Wu et al. (2005) have derived $\nabla_{\rm age} = 0.02 \pm 0.04$ (and scatter 0.25) and $\nabla_Z = -0.25 \pm 0.03$ (and scatter 0.19), which turn out to be qualitatively consistent again with our 'old' sample. The inclusion of dust extinction leaves our general considerations unaffected, as we will show in Appendix B5. The average trends of the metallicity and age gradients are almost unchanged, with variations going in the direction of a better match with other literature data.

The massive ETGs, with young cores ($<$6 Gyr) have very steep metallicity gradients, which are discrepant with respect to the literature results we have compared with. In Appendix A2, we have checked that this result does not depend on the contamination of the ETG sample from late-type systems. These latter, indeed, also show the same dependence of gradients on central age (see Fig. 4). A clear example of systems with very steep gradients is the isolated galaxy NGC 821 which have a young central stellar population and a metallicity gradient of $\nabla_Z = -0.72 \pm 0.04$ or NGC 2865, for which $\nabla_Z = -0.47 \pm 0.05$ (Proctor et al. 2005; Reda et al. 2007). One reason why we have been able to pick up this difference between centrally old and young systems is that most of the samples analysed in literature are made up of cluster ellipticals (e.g. Mehlert et al. 2003; Rawle et al. 2010), with only few cases of field galaxies (Ogando et al. 2005; Reda et al. 2007), while our sample is composed by galaxies living in various environments. On average, field galaxies are found to be younger and have a wider distribution of galaxy age (Bernardi et al. 1998; Trager et al. 2000; Thomas et al. 2005), thus a large fraction of our centrally young galaxies would be made of systems in the field or low-density environments with steeper age and metallicity gradients than those in cluster galaxies (due to the little interactions with the neighbourhood, see Section 3.2 and La Barbera et al. 2005). Note that the effect of the environment on colour and stellar population gradients is still debated with no conclusive results (e.g. Tamura et al. 2000; Tamura & Ohta 2000, 2003; Welikala et al. 2008, 2009).

Fig. 5 displays a relevant anticorrelation between age and metallicity gradients: for ETGs, the correlation is clear with a slope of -0.94 ± 0.02, while for LTGs it seems poorer but still significant, with a slope -0.48 ± 0.03 (see also Table 2). This is an intrinsic property of the galaxy sample, which is consistent with predictions from the galaxy merging scenario (e.g. Hopkins et al. 2009a) and with other observational evidences (e.g. Rawle et al. 2010). It is not spuriously induced by the well-known age–metallicity degeneracy (see Appendix B). In particular, galaxies with strong negative metallicity gradients have positive age gradients (coherently with the merging simulation in the figure), while the occurrence of nega-
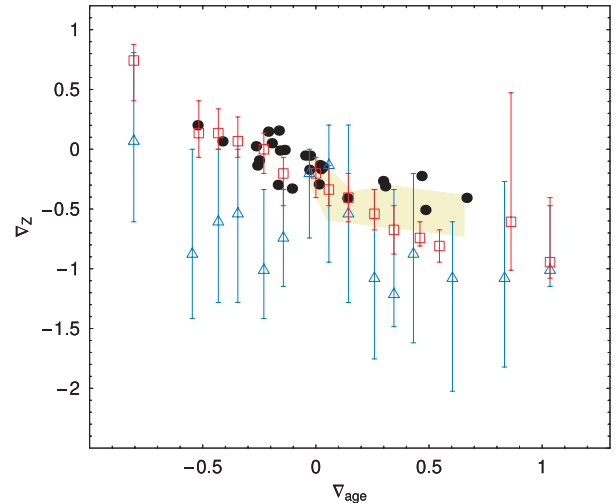

Figure 5. Metallicity versus age gradients for ETGs and LTGs. The symbols are the same as in Figs 2 and 4. Metallicity versus age gradients for ETGs are compared with predictions from gas-rich mergings in Hopkins et al. (2009a) (yellow shaded region) and cluster ETGs in Rawle et al. (2010) (black points).

tive age gradients is associated to small mass systems with positive metallicity gradients. The negative correlation found for LTGs is also qualitatively consistent with the literature on spiral galaxies (MacArthur et al. 2004).

In Fig. 6, we finally show the correlations between gradients and stellar parameters at different galaxy radii, with their related slopes listed in Table 2. Metallicity and age gradients show a tight correlation with central metallicity and age, respectively. For the ETGs, the age gradients are generally different from zero, positive for small central ages and null or negative for old systems. Metallicity gradients are negative for systems with older stellar populations at $R_{\rm eff}$ or with higher metallicity, while they are about zero for systems with old central ages or intermediate ages at $R_{\rm eff}$ (4–7 Gyr). Noticeably, the very positive ∇_Z and negative $\nabla_{\rm age}$ correspond to very young populations at $R_{\rm eff}$, i.e. recent SF outside the galaxy cores. These latter systems seem compatible with dwarf galaxies hosting expanding shells (e.g. Mori et al. 1997, see also Section 4).

Similarly, LTGs have also positive age gradients in presence of young cores, but in these cases we observe also large central metallicities (see Fig. 6, top row, third panel from left) and for these systems we also found the strongest metallicity gradients (bottom row, third panel of Fig. 6).

Overall, results in Figs 4 and 6 are in substantial agreement with the correlations reported in Rawle et al. (2010),[7] and with the findings in hydrodynamical simulations of both elliptical and disc galaxies (Hopkins et al. 2009a; Sánchez-Blázquez et al. 2009).

---

[7] In particular, if we limit our galaxies sample to luminous systems ($r < -20$ mag) with $Z_1 \geq 0.008$ and $age_1 \geq 2$ Gyr and perform the fit with respect to the central quantities within $R_{\rm eff}/3$, we find that the slope of the ∇_Z–$\log Z_1$ relation is -0.58 ± 0.04 in good agreement with the values in the range [−0.6, −0.7] from Rawle et al. (2010). For $\nabla_{\rm age}$–$\log age_1$ relation, we find a slope of -0.90 ± 0.06, which disagree with the shallower values reported in Rawle et al. (2010). A similar disagreement is found for the ∇_Z–$\log age_1$ and $\nabla_{\rm age}$–$\log Z_1$ correlations, where we find slopes 0.67 ± 0.05 and 0.50 ± 0.03 respectively, which are still not perfectly consistent with their results. These might be related to the small sample adopted, to the selected environment (i.e. cluster cores), to differences in population markers (i.e. line strengths rather than colours) and the use of synthetic spectral models with variable α enhancement overabundance.

Table 2. Slopes of the linear correlations between stellar population gradients ∇_Z, ∇_{age}, Z and age for ETGs and LTGs. IN and OUT indicate gradients correlated with inner (at $R = R_1$) and outer (at $R = R_2$) metallicity and age. In the last row the result for correlation between ∇_Z and ∇_{age} are reported. The fitting procedure is the same as that in Table 1.

Correlation	γ_{ETG}		γ_{LTG}	
	IN	OUT	IN	OUT
$\nabla_{age}-\log(age)$	-0.80 ± 0.03	0.93 ± 0.03	-0.78 ± 0.02	0.75 ± 0.03
$\nabla_{age}-\log Z^{(*)}$	0.09 ± 0.01	-0.34 ± 0.01	0.21 ± 0.01	-0.24 ± 0.02
$\nabla_Z-\log(age)$	0.62 ± 0.05	-1.07 ± 0.04	-0.20 ± 0.06	-0.62 ± 0.04
$\nabla_Z-\log Z$	-0.64 ± 0.02	0.06 ± 0.02	-0.49 ± 0.01	0.66 ± 0.02
$\nabla_Z-\nabla_{age}$	-0.92 ± 0.02		-0.50 ± 0.03	

* Here the linear correlation is a zeroth-order approximation.
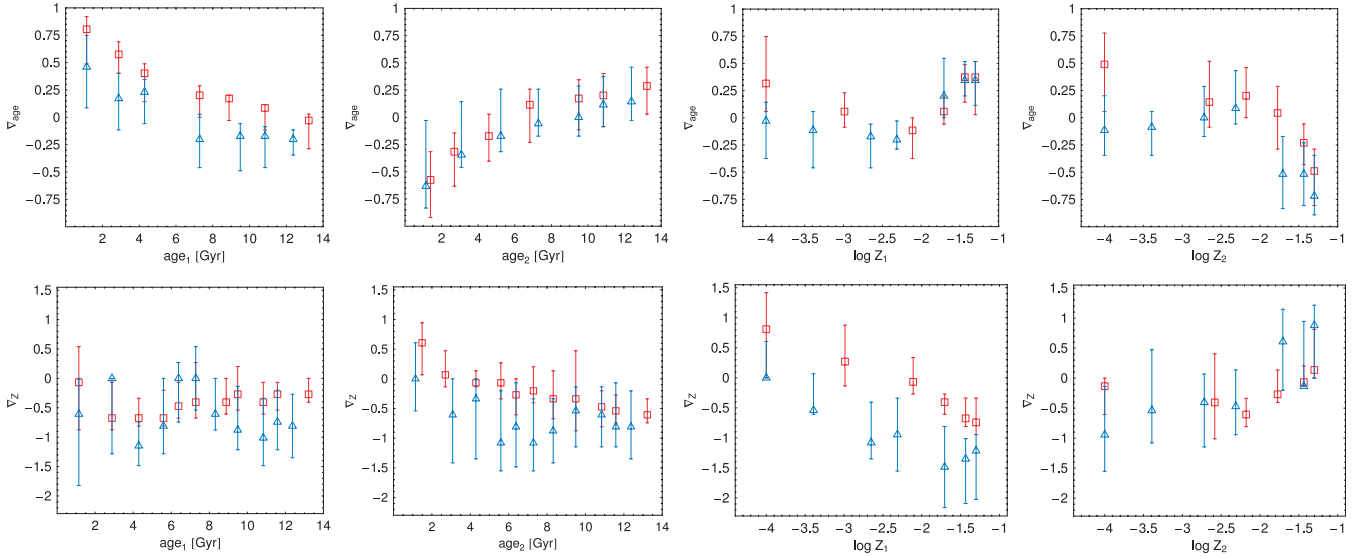
Figure 6. Correlations of gradients and fitted stellar parameters. The symbols are the same as in Figs 2, 4 and 5. Top panels: (from left) age gradient as a function of age_1, age_2, Z_1 and Z_2. Bottom panels: (from left) metallicity gradient as a function of age_1, age_2, Z_1 and Z_2.

3.4 Comparison with literature data

We now proceed to a more detailed comparison of our findings with a set of literature works which make use of a more sophisticated analysis, although usually associated to smaller samples. In particular, we concentrate on the ETG sample, taking the results for LTGs with the necessary caution, due to the larger degree of uncertainties arising from, e.g. (1) the simple assumption on the SF recipe, (2) the assumption of no dust gradients (see also Appendix B5) and (3) the prediction from theoretical simulations of the formation of such composite and complex systems which are still in their infancy (MacArthur et al. 2009; Martínez-Serrano et al. 2009; Sánchez-Blázquez et al. 2009).

Due to our minimal choice of the wavelength baseline and the possible biases on the stellar population estimates caused by the use of the optical band only, the comparison of our results with literature data is critical to (1) ultimately check the robustness of our results on the regions of the parameter space overlapping with independent analysis and (2) assess the gain in the physical information allowed by our analysis. In Fig. 7, we summarize the metallicity and age gradients for ETGs as a function of central velocity dispersion, and compare these with the observed gradients from a collection of literature studies (Mehlert et al. 2003; Proctor 2003; Ogando et al. 2005; Reda et al. 2007; Sánchez-Blázquez et al. 2007; Koleva et al. 2009a,b; Spolaor et al. 2009; Rawle et al. 2010). In the next

section, we will expand this comparison to the predictions from cosmological simulations. When considering massive ETGs, our ∇_Z are systematically steeper than literature data (see top left of Fig. 7), although showing on average a lower scatter than dwarf galaxies.

As seen in Fig. 6 and also illustrated in Fig. 7 (top-right panel), a significant contribution to the scatter of the metallicity gradients is linked to the age of galaxy cores, with older galaxies having, on average, shallower gradients than younger systems. When considering objects with $age_1 > 6$ Gyr, the agreement with the other studies (generally dealing with old systems; see Section 3.3) is remarkably good. The same conclusion is reached when considering the ∇_{age} (Fig. 7, bottom right), where the steeper (positive) gradients are shown by the younger systems. In Appendix B5, we show that shallower age gradients might be found if the dust extinction is accounted in the stellar models for the massive ETGs, while metallicity gradients remain almost unchanged.

The dependence of the gradients on the galaxy age is consistent with results in the dwarf regime by Spolaor et al. (2009) and Koleva et al. (2009a,b), which find shallower (and tightly correlated with mass) and steeper gradients in old and young systems, respectively. A similar spread in metallicity gradients is found in Chilingarian (2009).

As a final remark, galaxies with very low velocity dispersion ($\log \sigma_0 \lesssim 1.85$ km s^{-1}, see the vertical dashed grey line in Figs 7
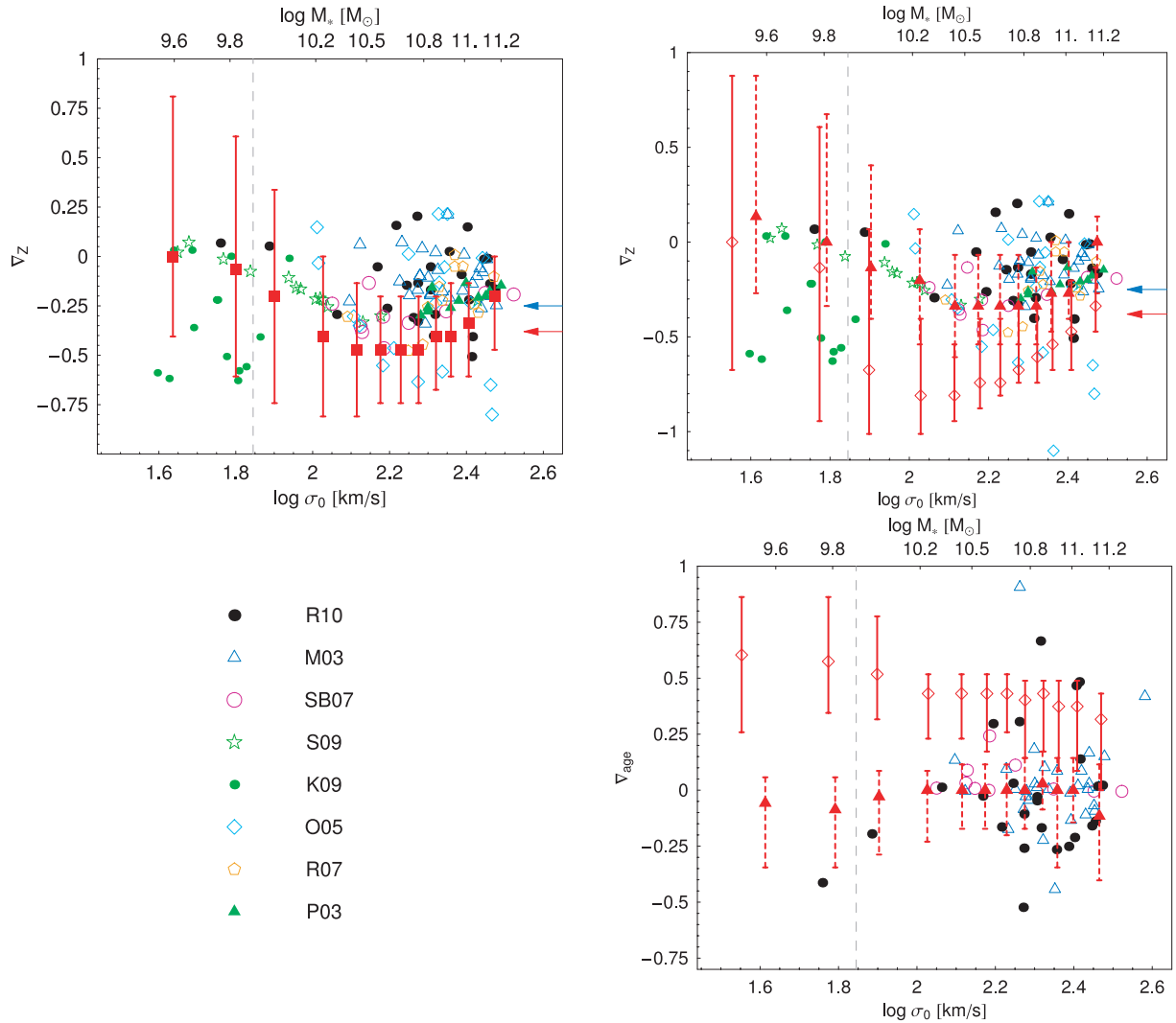
Figure 7. Metallicity gradients for ETGs as a function of central velocity dispersion compared with some literature data. Galaxies with velocity dispersion $\lesssim 70 \, \mathrm{km \, s^{-1}}$, at the left of the vertical dashed grey line, are somehow uncertain. Top left: metallicity gradients are compared with Rawle et al. (2010) (R10) as black points (including the results for Shapley and A3389 clusters), Mehlert et al. (2003) (M03) as blue triangles, Sánchez-Blázquez et al. (2007) (SB07) as purple circles, Spolaor et al. (2009) (S09) as green stars, Koleva et al. (2009a,b) (K09) as light green points, Ogando et al. (2005) (O05) as cyan diamonds, Reda et al. (2007) (R07) as orange pentagons and Proctor (2003) (P03) as green triangles. The blue and red arrows are for the results in Wu et al. (2005) and La Barbera & de Carvalho (2009). Top right: our ETGs divided in young and old central ages are compared with literature data: diamonds with continue bars are for ETGs with $0 < \mathrm{age}_1 \leq 6 \, \mathrm{Gyr}$; triangle with dashed bars are for $\mathrm{age}_1 > 6 \, \mathrm{Gyr}$. Bottom left: legend of symbols for literature data. Bottom right: age gradients divided by age are plotted versus literature data (M03, SB07 and R10) as above.

and 8) could be affected by some systematics due to the low signal-to-noise ratio and instrumental resolution of SDSS spectra. Notwithstanding this caution, our recovered gradients reproduce fairly well the literature results for dwarf ETGs (e.g. Spolaor et al. 2009). Also, the indication of shallower gradients at the lowest σ_0 seems robust, due to the clear turnover at $\log \sigma_0 \sim 2.2 \, \mathrm{km \, s^{-1}}$ and the inversion in the range $1.85 \lesssim \log \sigma_0 \lesssim 2.2 \, \mathrm{km \, s^{-1}}$.

4 DISCUSSION

Our results seem to support the idea that the metallicity trend versus the stellar mass for LTGs is mainly driven by the interplay of gas inflow and winds from SNe and evolved stars (Matteucci 1994; Kobayashi 2004; Pipino et al. 2008). These processes tend to increase the central metallicity and prevent the enrichment of the outer regions. Therefore more massive systems have on aver-

age larger central metallicities which correspond to steeper negative gradients.

Low-mass ETGs ($M_* \lesssim 10^{10.3}$–$10^{10.5} \, \mathrm{M_\odot}$, see Table 1) show a similar correlation of the metallicity gradient with stellar mass (Fig. 4), which suggests that they might experience the effect of infall/SN feedback as LTGs. For instance, low-mass ETGs in Fig. 8 are consistent with SN feedback (both soft and strong), as predicted in chemodynamical simulations in Kawata (2001). On average, weaker SN feedback gives gradients in agreement with ours at intermediate $\log \sigma_0 (\sim 2.2 \, \mathrm{km \, s^{-1}})$, while the stronger feedback recipe seems to reproduce better the low $\log \sigma_0$ side of the correlation. A recipe including the SN feedback with a varying power as a function of mass (Dekel & Silk 1986; Dekel & Birnboim 2006) would allow a fairly good match of the observed decreasing trend of the gradients for the less massive galaxies (as in Kawata & Gibson 2003), but it fails to reproduce our observed gradients for the very massive
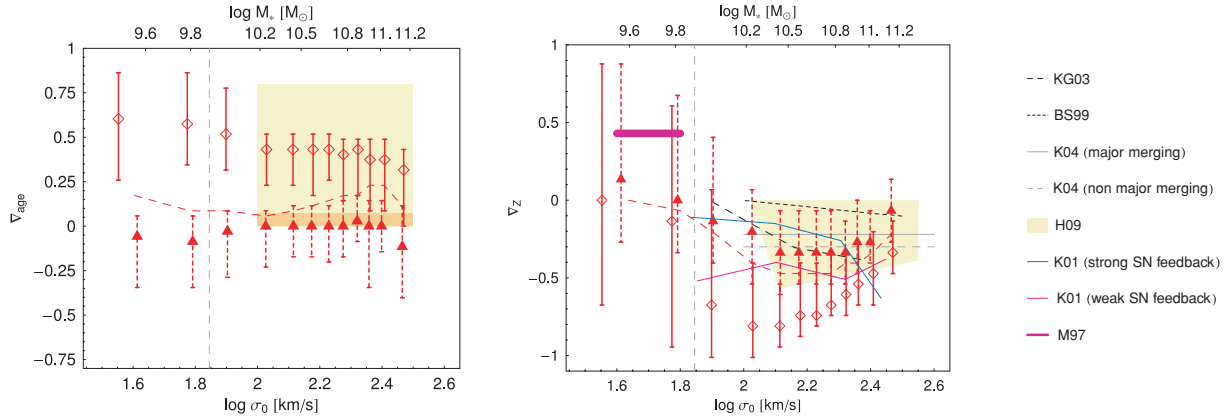
Figure 8. Left: age gradients versus simulations. Comparison with gas-rich merging predictions in Hopkins et al. (2009a) (H09), with the darker (lighter) region showing galaxies older (younger) than 6 Gyr. Middle: metallicity gradients versus simulations. The predictions from merging models in Bekki & Shioya (1999) (BS99) are shown as short dashed line, dissipative collapse models in Kawata & Gibson (2003) (KG03) as long dashed line, the remnants of major mergings between gas-rich disc galaxies in Hopkins et al. (2009a) as yellow shaded region, the typical gradient for major (continue grey line) and non-major (dashed grey line) mergings in Kobayashi (2004) (K04); The violet thick line shows the predictions as in the simulation of Mori et al. (1997) (M97); blue and pink lines are the result from the chemodynamical model in Kawata (2001) (K01), respectively, for strong and weak SNe feedback models (the *B*-band magnitude in this work is transformed in a velocity dispersion σ_0 using the relation in Tortora et al. 2009a). The symbols are as in Fig. 7 and the dashed red line is for the whole ETGs sample. Right: symbol legend for simulations.

systems. Moreover, as seen in Fig. 4, the absolute value of ∇_Z of ETGs is lower than for the LTGs, probably as a consequence of the dilution of the gradient due to the higher density environment where ETGs generally live in (see also discussion in Section 3.2). It might be also the effect of other mechanisms at work such as merging (see, e.g. Kobayashi 2004), which however is expected to be less effective in these mass ranges (de Lucia et al. 2006).

At very low masses ($M_* \lesssim 10^{9.5}\,M_\odot$ and $\log \sigma_c \lesssim 1.8\,\mathrm{km\,s^{-1}}$), the ∇_Z turns to even positive values, which mainly corresponds to systems with negative ∇_{age} as in Fig. 5 and very low central metallicities as in Fig. 6; these dwarf-like systems are compatible with the expanding shell model from Mori et al. (1997) (see also Fig. 8).

At larger masses, the shallow metallicity gradients of ETGs suggest that these have experienced merging and/or tidal interactions (at a rate that could increase as a function of the stellar mass) which have diluted the ∇_Z. Such events might have taken place in earlier phases of the galaxy evolution, as indicated by the presence of null age gradients in old systems. In Fig. 8, we compare the ∇_{age} with the prediction from the hierarchical simulations in Hopkins et al. 2009a, where a perfect agreement is found for the old sample (see also the good agreement with literature data in Fig. 7). From the same simulations, we also see that systems with younger cores are expected to show positive gradients which are fully consistent with our low central age systems as in Fig. 4 and also reported in Fig. 8. In the same figure, metallicity gradients are in qualitative agreement with gradients of remnants in Hopkins et al. (2009a) and the medians from Kobayashi (2004), while the merging models in Bekki & Shioya (1999) reproduce the mean gradients in galaxies with $\log \sigma_0 \gtrsim 2.4$, but fail at lower σ_0. Once again, if we consider the older systems only, they are in a better agreement with the merging simulations: this is expected since, after the initial gas rich-merging events that might produce both a larger central metallicity and a positive age gradient (Kobayashi 2004; Mihos & Hernquist 1994), subsequent gas poor-merging may dilute the positive age gradient with time as well as make the metallicity gradients to flatten out (White 1980; Di Matteo et al. 2009; Hopkins et al. 2009a) – see also left column of Fig. 6. In this respect, massive and old ETG systems

seem to be fully consistent with the merging scenario. However, a further mechanism that may act to produce the shallower (or almost null) colour and metallicity gradients in old massive ETGs, with $M_* \gtrsim 10^{11}\,M_\odot$ and $\log \sigma_0 \gtrsim 2.4$ (Fig. 4), might be due to the strong quasar feedback at high redshift (Tortora et al. 2009b), while steeper metallicity gradients at lower masses could be linked to less efficient AGNs.

5 CONCLUSIONS

We have investigated the CGs in a sample of ∼50 000 local galaxies from the SDSS as a function of structural parameters, luminosity and stellar mass. CGs have been found to correlate mainly with luminosity and stellar mass. They have a negative minimum ($\nabla_{g-i} \sim -0.2$) at $M_* \sim 10^{10.3}\,M_\odot$, and increase with the mass for $M_* \gtrsim 10^{10.3}\,M_\odot$, the very massive galaxies, $M_* \gtrsim 10^{11}\,M_\odot$, having the shallower values (~ -0.1). On the other mass side, the gradients decrease with mass and become positive for $M_* \lesssim 10^9\,M_\odot$. These trends are mirrored by similar behaviours with luminosity and galaxy size, e.g. the gradients have a minimum at $r \sim -20$ mag and $\log R_{\mathrm{eff}} \sim 0.5$, then increase towards the small and the large end of the parameter distribution, turning to positive values for $\log R_{\mathrm{eff}} \lesssim 0$ and $r \gtrsim -18$ mag. The dependence on velocity dispersion is very loose. A clear dichotomy is also found when looking at the dependence on the Sérsic index n which suggests a distinct behaviour between the ETG and LTG. In fact, these two families mark clear differences in their trends with structural parameters (e.g. mass and σ_0).

For LTGs, ∇_{g-i} monotonically decreases with the mass, with more massive systems having the lowest CGs (~ -0.4) and less massive systems ($M_* \lesssim 10^8$–$10^{8.5}\,M_\odot$) showing even positive gradients. ETGs have negative gradients mildly increasing with mass for $\log M_* \gtrsim 10^{10.3}$–$10^{10.5}\,M_\odot$, which marks the mass scale for the gradient slope inversion (see Table 1). This result is consistent with Spolaor et al. (2009) and reminiscent of the typical mass scale where the SF and structural parameters in galaxies drastically change (Capaccioli et al. 1992a,b; Kauffmann et al. 2003; Croton et al. 2006; Cattaneo et al. 2008). A similar trend is observed when plotting

the gradients as a function of effective radius, while a tighter trend with velocity dispersion is evident for ETGs only (Fig. 4). This was masked when plotting LTGs and ETGs together.

We have used galaxy colours at $0.1R_{eff}$ and $1R_{eff}$ in our synthetic spectral models to determine the variation of age and metallicity at these radii. The observed trends of the CGs with mass and σ_0 are correlated with a similar trends for metallicity and age gradients. Despite the large scatter of the data, the strong correlation of metallicity gradients with the central velocity dispersion of ETGs is clear, with a turnoff point at $\log \sigma_0 \sim 2.2 \, \mathrm{km \, s^{-1}}$ (see Table 1). These results are in very good agreement with a collection of results from literature (Mehlert et al. 2003; Proctor 2003; Ogando et al. 2005; Reda et al. 2007; Sánchez-Blázquez et al. 2007; Koleva et al. 2009a,b; Rawle et al. 2010; Spolaor et al. 2009), in particular for the old galaxies in our sample.

A remarkable result of our analysis is the confirmation that the galaxy (central) age is one of the main drivers of the scatter of the age and metallicity gradients, with the older systems showing generally the shallower gradients with respect the young ones. In Fig. 7, for instance, we show that in the low-mass regime, at fixed σ_0, older galaxies have on average shallower gradients, consistently with the results in Spolaor et al. (2009), while systems with late formation or with a recent SF episode have a larger spread (and metallicity gradients down to very low values, ~ -0.6), consistently with findings in Koleva et al. (2009a,b). The measured scatter (see also Chilingarian 2009 for a similar spread) might be the consequence of a variety of phenomena affecting the dwarf galaxy evolution, such as (soft) SN feedback, interaction/merging in the high-density environment and SF by shell expansion (Fig. 8). On the other mass side, a further factor of the spread of the massive systems gradients might be the randomness of the initial conditions of the mergings (Rawle et al. 2010).

Previous attempts to quantify the correlations of gradients with luminosity, mass or velocity dispersion have often failed, mainly because of the exiguity of the galaxy sample (e.g. Peletier et al. 1990a; Kobayashi & Arimoto 1999; Tamura & Ohta 2003). Only recently, a clear correlation of the colour and metallicity gradients with mass has been ascertained (see e.g. Forbes et al. 2005), pointing to different trends for high- and low-mass galaxies (Rawle et al. 2010; Spolaor et al. 2009). Our analysis has confirmed and reinforced these results, as it relies on one of the largest local galaxy samples including dwarf and ordinary galaxies. Using CGs derived by the structural parameters in B05, we obtained statistically meaningful trends, which allow us to fix the link with physical phenomena as well as to make direct comparisons with predictions from simulations (Mori et al. 1997; Bekki & Shioya 1999; Kawata 2001; Kawata & Gibson 2003; Kobayashi 2004; Hopkins et al. 2009a).

We can finally draw the physical scenario sketched in Fig. 9, resting on the results discussed so far. The formation of LTGs and less massive ETGs is mainly driven by a monolithic-like collapse as they have almost null or positive age gradients and negative metallicity gradients decreasing with the mass. These are in fact well explained by simple gas inflow and feedback from SN and evolved stars, and also reproduced in simulations of dissipative collapse and SN feedback models in Fig. 8 (Larson 1974, 1975; Carlberg 1984; Arimoto & Yoshii 1987; Kawata & Gibson 2003). The difference in the magnitude of the gradients between LTGs and lower mass ETGs mainly resides in the effect of the environment as the former live in very low density environments, while the latter stay in massive haloes, together with more massive ETGs. Here they experience strong gravitational interactions producing shallower colour and metallicity gradients. The efficiency of such
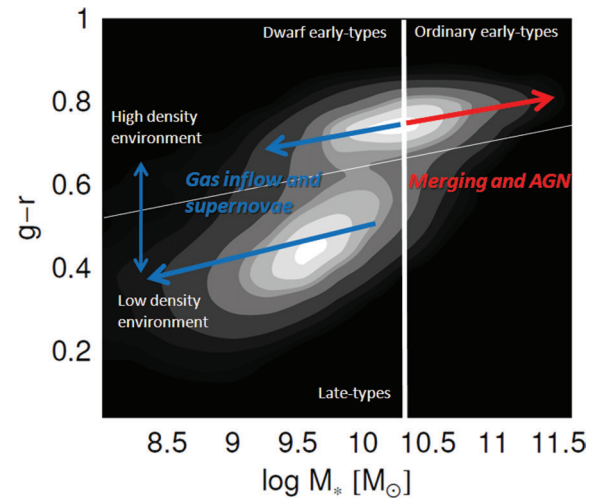

Figure 9. Colour–mass diagram. The contours show the density of data points with grey-scale going from darker (low density of galaxies) to brighter regions (high density). The thin white line sets the separation between RS and BC; the thick vertical one gives the mass scale, $M_* \sim 10^{10.3}$, which separates galaxies belonging to the RS in normal and dwarf ETGs, and sets a qualitative upper mass for LTGs. The arrows give information about the efficiency of the phenomena which drive the twofold trend we discuss in the paper. AGN feedback and merging are important at high mass with an efficiency increasing with mass, while SN feedback and gas inflow drive the galaxy evolution in the less massive side, with an efficiency that is larger at the lowest masses. Galaxies in RS and BC lie in environments with a different density, which is manifested as a difference of the gradients in the two samples.

phenomena is strong enough for lower mass ETGs, thus shaping the observed decreasing trend with mass (see e.g. Dekel & Birnboim 2006).

The most massive ETG systems have shallower gradients (Bekki & Shioya 1999; Kobayashi 2004; Hopkins et al. 2009a), flattening out with the mass due to the increasing intervention of (gas-rich and -poor) merging, tidal interactions and quasar/radio mode AGN feedback (Capaccioli et al. 1992a; Ferrarese & Merritt 2000; de Lucia et al. 2006; Dekel & Birnboim 2006; Liu, Jiang & Gu 2006; Sijacki et al. 2007; Cattaneo et al. 2008). All the simulations collected in literature fail to reproduce the fine details of the trends we find, suggesting that a full understanding of physical processes involved in the galaxy evolution is still missing.

In future analysis, we plan to enlarge the wavelength baseline and also to use line-strength measurements for the stellar model (when available). We will investigate the systematics induced when other synthetic prescriptions are assumed and the dependence of the CGs on the galaxy SF history. We will derive the *M/L* gradients, if any, and discuss their impact on the dark matter content of ETGs and correlate the CGs with the DM fraction of these systems as probe of the galaxy potential wells. Finally, the realization of hydrodynamical simulations of jets emitted by AGN would be useful to shape, together with galaxy merging, the colour and metallicity gradients for massive galaxies.

REFERENCES

Allen P. D., Driver S. P., Graham A. W., Cameron E., Liske J., De Propris R., 2006, MNRAS, 371, 2
Antonuccio-Delogu V., Silk J., 2008, MNRAS, 389, 1750
Arimoto N., Yoshii Y., 1987, A&A, 173, 23
Balcells M., Peletier R. F., 1994, AJ, 107, 135
Baldry I. K., Glazebrook K., Driver S. P., 2008, MNRAS, 388, 945
Bakos J., Trujillo I., Pohlen M., 2008, ApJ, 683, 103
Bekki K., Shioya Y., 1999, ApJ, 513, 108
Bell E. F., de Jong R. S., 2001, ApJ, 550, 212
Bender R., Surma P., Döbereiner S., Möllenhoff C., Madejsky R., 1989, A&A, 217, 35
Bernardi M., Renzini A., de Costa L. N., Wegner G., Alonso M. V., Pellegrini P. S., Rité C., Willmer C. N. A., 1998, ApJ, 508, 143
Blanton M. R. et al., 2003a, AJ, 125, 2348
Blanton M. R. et al., 2003b, ApJ, 592, 819
Blanton M. R., Lupton R. H., Schlegel D. J., Strauss M. A., Brinkmann J., Fukugita M., Loveday J., 2005a, ApJ, 631, 208
Blanton M. R. et al., 2005b, AJ, 129, 2562 (B05)
Brammer G. B. et al., 2009, ApJ, 706, L173
Bruzual A. G., Charlot S., 2003, MNRAS, 344, 1000 (BC03)
Bundy K. et al., 2006, ApJ, 651, 120
Burstein D., Faber S. M., Gaskell C. M., Krumm N., 1984, ApJ, 287, 586
Cameron E., Driver S. P., Graham A. W., Liske J., 2009, ApJ, 699, 105
Caon N., Capaccioli M., D'Onofrio M., 1993, MNRAS, 265, 1013
Capaccioli M., Caon N., D'Onofrio M., 1992a, MNRAS, 259, 323
Capaccioli M., Caon N., D'Onofrio M., 1992b, in Danziger J., Zeilinger W. W., Kjar K., eds, ESO ESP/EIPC Workshop, Structure, Dynamics and Chemical Evolution of Early-type Galaxies (Elba). ESO, Garching, p. 43
Capozziello S., Cardone V. F., Molinaro R., Salzano V., 2007, preprint (astro-ph/0703532)
Cappellari M. et al., 2006, MNRAS, 366, 1126
Cardelli J. A., Clayton G. C., Mathis J. S., 1989, ApJ, 345, 245
Cardiel N., Gorgas J., Sánchez-Blázquez P., Cenarro A. J., Pedraz S., Bruzual G., Klement J., 2003, A&A, 409, 511
Carlberg R. G., 1984, ApJ, 286, 403
Carollo C. M., Danziger I. J., Buson L., 1993, MNRAS, 265, 553
Cattaneo A., Dekel A., Devriendt J., Guiderdoni B., Blaizot J., 2006, MNRAS, 370, 1651
Cattaneo A., Dekel A., Faber S. M., Guiderdoni B., 2008, MNRAS, 389, 567
Cattaneo A., Mamon G. A., Warnick K., Knebe A., 2010, preprint (arXiv:1002.3257)
Chaboyer B., 1994, in Meylan G., Prugniel P., eds, ESOyOHP Workshop on Dwarf Galaxies. ESO, Garching, p. 485
Chabrier G., 2001, ApJ, 554, 1274
Chabrier G., 2002, ApJ, 567, 304
Chabrier G., 2003, PASP, 115, 763
Chang R., Gallazi A., Kauffmann G., Charlot S., Ivezic Z., Brinchmann J., Heckman T. M., 2006, MNRAS, 366, 717
Chilingarian I. V., 2009, MNRAS, 394, 1229
Chiosi C., Carraro G., 2002, MNRAS, 335, 335
Cimatti A., Daddi E., Renzini A., 2006, A&A 453, L29
Conroy C., Gunn J. E., 2010, ApJ, 712, 833
Conroy C., Wechsler R. H., 2009, ApJ, 696, 620
Conroy C., Gunn J. E., White M., 2009, ApJ, 699, 486
Conroy C., Gunn J. E., White M., 2010, ApJ, 708, 58
Cowie L. L., Songaila A., Hu E. M., Cohen J. G., 1996, AJ, 112, 839
Croton D. J. et al., 2006, MNRAS, 365, 11
Daddi E. et al., 2005, ApJ, 626, 680
Dalcanton J. J., Bernstein R. A., 2002, AJ, 124, 1328

Davies R. L., Sadler E. M., Peletier R. F., 1993, MNRAS, 262, 650
de Jong R. S., 1996, A&A, 313, 377
de Lucia G., Springel V., White S. D. M., Croton D., Kauffmann G., 2006, MNRAS, 366, 499
Dekel A., Birnboim Y., 2006, MNRAS, 368, 2
Dekel A., Silk J., 1986, ApJ, 303, 39
Dorman B., O'Connell R. W., Rood R. T., 2003, ApJ, 591, 878
Drory N., Alvarez M., 2008, ApJ, 680, 41
di Matteo T., Springel V., Hernquist L., 2005, Nat, 433, 604
Di Matteo P., Pipino A., Lehnert M. D., Combes F., Semelin B., 2009, A&A, 499, 427
Ferrarese L., Merritt D., 2000, ApJ, 539, 9
Fontanot F., De Lucia G., Monaco P., Somerville R. S., Santini P., 2009, MNRAS, 397, 1776
Forbes D. A., Sánchez-Blázquez P., Proctor R., 2005, MNRAS, 361, 6
Franx M., Illingworth B., Heckman T., 1989, AJ, 98, 538
Gallazzi A., Charlot S., Brinchmann J., White S. D. M., Tremonti C. A., 2005, MNRAS, 362, 41
Ganda K. et al., 2007, MNRAS, 380, 506
Gibson B. K., 1997, MNRAS, 290, 471
Glazebrook K. et al., 2004, Nat, 430, 181
Goudfrooij P., de Jong T., 1995, A&A, 298, 784
Graham A. W., Guzmán R., 2003, AJ, 125, 2936
Graham A. W., Erwin P., Trujillo I., Asensio Ramos A., 2003, AJ, 125, 2951
Graham A. W., Driver S. P., Petrosian V., Conselice C. J., Bershady M. A., Crawford S. M., Goto T., 2005, AJ, 130, 1535
Guo Y. et al., 2009, MNRAS, 398, 1129
Henry R. B. C., Worthey G., 1999, PASP, 111, 919
Hopkins P. F., Cox T. J., Dutta S. N., Hernquist L., Kormendy J., Lauer T. R., 2009a, ApJS, 181, 135
Hopkins P. F., Lauer T. R., Cox T. J., Hernquist L., Kormendy J., 2009b, ApJS, 181, 486
Jansen R. A., Franx M., Fabricant D., Caldwell N., 2000, ApJS, 126, 271
Jarrett T. H., Chester T., Cutri R., Schneider S. E., Huchra J. P., 2003, AJ, 125, 525
Jimenez R., Panter B., Heavens A. F., Verde L., 2005, MNRAS, 356, 495
Jørgensen I., Franx M., Kjærgaard P., 1995, MNRAS, 273, 1097
Jørgensen I., Franx M., Kjærgaard P., 1996, MNRAS, 280, 167
Kannappan S. J., Gawiser E., 2007, ApJ, 657, 5
Kauffmann G., White S. D. M., 1993, MNRAS, 261, 921
Kauffmann G. et al., 2003, MNRAS, 341, 54
Kaviraj S., Kirkby L. A., Silk J., Sarzi M., 2007, MNRAS, 382, 960
Kawata D., 2001, ApJ, 558, 598
Kawata D., Gibson B. K., 2003, MNRAS, 340, 908
Kennicutt R. C., 1983, ApJ, 272, 54
Khalatyan A., Cattaneo A., Schramm M., Gottlber S., Steinmetz M., Wisotzki L., 2008, MNRAS, 387, 13
Kim K. O., Ann H. B., 1990, J. Korean Astron. Soc., 22, 43
Kobayashi C., 2004, MNRAS, 347, 740
Kobayashi C., Arimoto N., 1999, ApJ, 527, 573
Koleva M., De Rijcke S., Prugneil Ph., Zeilinger W. W., Michielsen D., 2009a, MNRAS, 396, 2133
Koleva M., Prugniel Ph., De Rijcke S., Zeilinger W. W., Michielsen D., 2009b, Astron. Nachr, 330, 960 (arXiv:0910.2643)
Kormendy J., Djorgovski S., 1989, ARA&A, 27, 235
Kormendy J., Fisher D. B., Cornell M. E., Bender R., 2009, ApJS, 182, 216
Kuntschner H. et al., 2006, MNRAS, 369, 497
La Barbera F., de Carvalho R. R., 2009, ApJ, 699, 76
La Barbera F., Busarello G., Merluzzi P., Massarotti M., Capaccioli M., 2002, ApJ, 571, 790
La Barbera F., Busarello G., Massarotti M., Merluzzi P., Mercurio A., 2003, A&A, 409, 21
La Barbera F., de Carvalho R. R., Gal R. R., Busarello G., Merluzzi P., Capaccioli M., Djorgovski S. G., 2005, ApJ, 626, 19
Larson R. B., 1974, MNRAS, 166, 585
Larson R. B., 1975, MNRAS, 173, 671
Lee J. H., Lee M. G., Kim T., Hwang H. S., Park C., Choi Y.-Y., 2007, ApJ, 663, 69

Li C., White S. D. M., 2009, MNRAS, 398, 2177

Li Z., Han Z., Zhang F., 2007, A&A, 464, 853

Lintott C. et al., 2008, MNRAS, 389, 1179

Liu Y., Jiang D. R., Gu M. F., 2006, ApJ, 637, 669

Liu C. Z., Shen S.-Y., Shao Z.-Y., Chang R.-X., Hou J.-L., Yin J., Yang D.-W., 2009, Res. Astron. Astrophys., 9, 1119

MacArthur L. A., 2005, ApJ, 623, 795

MacArthur L. A., Courteau S., Bell E., Holtzman J. A., 2004, ApJS, 152, 175

MacArthur L. A., González J. J., Courteau S., 2009, MNRAS, 395, 28

Maller A. H., Berlind A. A., Blanton M. R., Hogg D. W., 2009, ApJ, 691, 394

Maraston C., 2005, MNRAS, 362, 799

Maraston C., Strömbölack G., Thomas D., Wake D. A., Nichol R. C., 2009, MNRAS, 394, L107

Martínez-Serrano F. J., Serna A., Doménech-Moral M., Domínguez-Tenreiro R., 2009, ApJ, 705, 133

Matteucci F., 1994, A&A, 288, 57

Mehlert D., Thomas D., Saglia R. P., Bender R., Wegner G., 2003, A&A, 407, 423

Mihos J. C., Hernquist L., 1994, ApJ, 437, L47

Mori M., Yoshi Y., Tsujimoto T., Nomoto K., 1997, ApJ, 478, 21

Nakamura O., Fukugita M., Yasuda N., Loveday J., Brinkmann J., Schneider D. P., Shimasaku K., SubbaRao M., 2003, ApJ, 125, 1682

Napolitano N. R. et al., 2005, MNRAS, 357, 691

Napolitano N. R., Romanowsky A. J., Tortora C., 2010, preprint (arXiv:1003.1716)

Neistein E., van den Bosch F. C., Dekel A., 2006, MNRAS, 372, 933

Nelan J. E., Smith R. J., Hudson M. J., Wegner G. A., Lucey J. R., Moore S. A. W., Quinney S. J., Suntzeff N. B., 2005, ApJ, 632, 137

Ogando R. L. C., Maia M. A. G., Chiappini C., Pellegrini P. S., Schiavon R. P., da Costa L. N., 2005, ApJ, 632, 61

Padmanabhan N. et al., 2004, New Astron., 9, 329

Pannella M., Hopp U., Saglia R. P., Bender R., Drory N., Salvato M., Gabasch A., Feulner G., 2006, ApJ, 639, L1

Panter B., Jimenez R., Heavens A. F., Charlot S., 2007, MNRAS, 378, 1550

Park C., Choi Y.-Y., 2005, ApJ, 635, 29

Peletier R. F., Davies R. L., Illingworth G. D., Davis L. E., Cawson M., 1990a, AJ, 100, 1091

Peletier R. F., Valentijn E. A., Jameson R. F., 1990b, A&A, 233, 62

Peletier R. F. et al., 2007, MNRAS, 379, 445

Pipino A., Matteucci F., Borgani S., Biviano A., 2002, New Astron., 7, 227

Pipino A., D'Ercole A., Matteucci F., 2008, A&A, 484, 679

Proctor R. N., 2003, PhD Thesis, Univ. Central Lancashire

Proctor R. N., Forbes D. A., Forestell A., Gebhardt K., 2005, MNRAS, 362, 857

Prugniel P., Simien F., 1997, A&A, 321, 111

Rawle T. D., Smith R. J., Lucey J. R., 2010, MNRAS, 401, 852

Recchi S., Matteucci F., D'Ercole A., 2001, MNRAS, 322, 800

Reda F. M., Proctor R. N., Forbes D. A., Hau G. K. T., Larsen S. S., 2007, MNRAS, 377, 1772

Rettura A. et al., 2006, A&A, 458, 717

Romeo A. D., Napolitano N. R., Covone G., Sommer-Larsen J., Antonuccio-Delogu V., Capacciolli M., 2008, MNRAS, 389, 13

Ruszkowski M., Springel V., 2009, ApJ, 696, 1094

Saglia R. P., Maraston C., Greggio L., Bender R., Ziegler B., 2000, A&A, 360, 911

Salpeter E. E., 1955, ApJ, 121, 161

Sánchez-Blázquez P., Forbes D. A., Strader J., Brodie J., Proctor R., 2007, MNRAS, 377, 759

Sánchez-Blázquez P., Courty S., Gibson B. K., Brook C. B., 2009, MNRAS, 398, 591

Sandage A., 1972, ApJ, 176, 21

Scannapieco C., Tissera P. B., White S. D. M., Springel V., 2006, MNRAS, 371, 1125

Schawinski K., Thomas D., Sarzi M., Maraston C., Kaviraj S., Joo S.-J., Yi S. K., Silk J., 2007, MNRAS, 382, 1415

Schlegel D. J., Finkbeiner D. P., Davis M., 1998, ApJ, 500, 525

Scodeggio M., 2001, ApJ, 121, 2413

Shen S., Mo H. J., White S. D. M., Blanton M. R., Kauffmann G., Voges W., Brinkmann J., Csabai I., 2003, MNRAS, 343, 978

Shimasaku K. et al., 2001, AJ, 122, 1238

Sijacki D., Springel V., Di Matteo T., Hernquist L., 2007, MNRAS, 380, 877

Spergel D. N. et al., 2003, ApJS, 148, 175

Spergel D. N. et al., 2007, ApJS, 170, 377

Spolaor M., Proctor R. N., Forbes D. A., Couch W. J., 2009, ApJ, 691, 138

Strateva I. et al., 2001, AJ, 122, 1861

Suh H., Jeong H., Oh K., Yi S. K., Ferreras I., Schawinski K., 2010, ApJS, 187, 374

Tamura N., Ohta K., 2000, AJ, 120, 533

Tamura N., Ohta K., 2003, AJ, 126, 596

Tamura N., Kobayashi C., Arimoto N., Kodama T., Ohta K., 2000, AJ, 119, 2134

Taylor V. A., Jansen R. A., Windhorst R. A., Odewahn S. C., Hibbard J. E., 2005, ApJ, 630, 784

Thomas D., Maraston C., Bender R., Mendes de Oliveira C., 2005, ApJ, 621, 673

Tortora C., Napolitano N. R., Romanowsky A. J., Capacciolli M., Covone G., 2009a, MNRAS, 396, 1132

Tortora C., Antonuccio-Delogu V., Kaviraj S., Silk J., Romeo A. D., Becciani U., 2009b, MNRAS, 396, 61

Trager S. C., Faber S. M., Worthey G., Gonzalez J. J., 2000, AJ, 119, 1645

Treu T. et al., 2005, ApJ, 633, 174

Trujillo I. et al., 2004a, ApJ, 604, 521

Trujillo I., Erwin P., Asensio Ramos A., Graham A. W., 2004b, AJ, 127, 1917

Trujillo I. et al., 2006, ApJ, 650, 18

Tully R. B., Verheijen M. A. W., Pierce M. J., Huang J., Wainscoat R. J., 1996, AJ, 112, 2471

Vader J. P., Vigroux L., Lachièze-Rey M., Souviron J., 1988, A&A, 203, 217

van der Wel A., Franx M., Wuyts S., van Dokkum P. G., Huang J., Rix H.-W., Illingworth G. D., 2006, ApJ, 652, 97

Weinmann S. M., Kauffmann G., van den Bosch F. C., Pasquali A., McIntosh D. H., Mo H., Yang X., Guo Y., 2009, MNRAS, 394, 1213

Welikala N., Connolly A. J., Hopkins A. M., Scranton R., Conti A., 2008, ApJ, 677, 970

Welikala N., Connolly A. J., Hopkins A. M., Scranton R., 2009, ApJ, 701, 994

White S. D. M., 1980, MNRAS, 191, 1

Wise M. W., Silva D. R., 1996, ApJ, 461, 155

Worthey G., 1994, ApJS, 95, 107

Wu H., Shao Z., Mo H. J., Xia X., Deng Z., 2005, ApJ, 622, 244

APPENDIX A: SAMPLE SYSTEMATICS AND CONTAMINANTS

We analyse various systematics in the galaxy sample and in the selection criteria.

A1 Sample systematics

We quantify the effect of source incompleteness on our results, in particular on the age and metallicity gradients as a function of stellar mass.

Our sample is magnitude limited, and misses increasingly fainter and less massive galaxies at larger redshifts; e.g. at $z_{spec} = 0.02$, the lowest mass galaxies have $M_* \sim 10^{8.2}\,M_\odot$, while at $z_{spec} = 0.05$ this limit increases to $M_* \sim 10^9\,M_\odot$ (see Blanton et al. 2005a and the left-hand panel in Fig. A1). We already mentioned that dwarf galaxies can be missed due to surface brightness selection effects (photometric incompleteness). Other less obvious sources of incompleteness are defects in deblending and the absence of reliable redshift measurements.
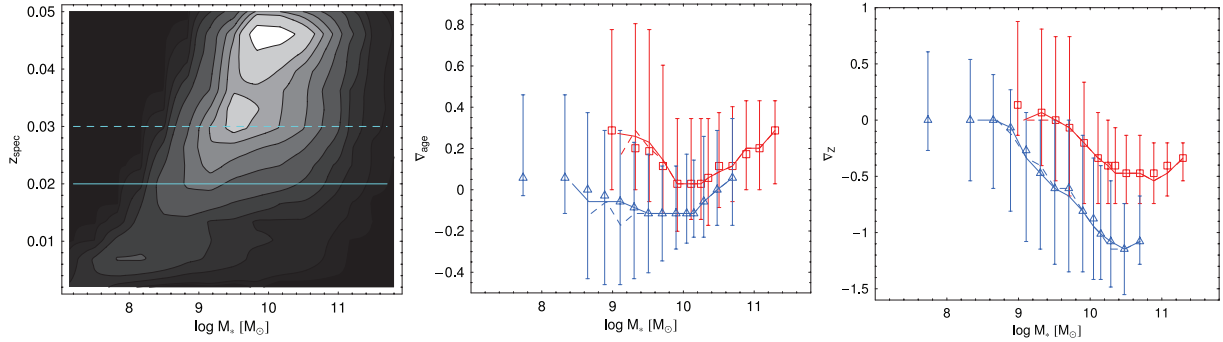
Figure A1. Left-hand panel: spectroscopic redshift as a function of stellar mass for the B05 galaxy sample. The two lines are relative to the redshift thresholds we use to select subsamples of galaxies. Middle panel: age gradients as a function of stellar mass. Right-hand panel: metallicity gradients as a function of stellar mass. The red and blue symbols with bars are relative to the full galaxy sample for ETGs and LTGs respectively, as discussed in the text, and the continue and dashed lines are for subsamples with $z_{\rm spec} > 0.02$ and $z_{\rm spec} > 0.03$.

By analysing the surface brightness completeness of this sample of galaxies, Blanton et al. (2005a) found that for $r < -18$ mag ($M_* \lesssim 10^9\,{\rm M_\odot}$) the catalogue is complete at more than 90 per cent, while at fainter magnitudes the photometric pipeline could mistakenly deblend galaxies or overestimate the background sky level. However, down to $M_* \sim 10^{8.5}\,{\rm M_\odot}$ the overall incompleteness is not dramatic (Blanton et al. 2005a; Baldry et al. 2008; Li & White 2009). Moreover, at $z_{\rm spec} \lesssim 0.02$ the distribution of galaxies seems patchy and the fraction of massive galaxies with $M_* \gtrsim 10^9\,{\rm M_\odot}$ turns out to be smaller, and not homogeneously distributed as the one at larger redshifts. In order to account for all possible biases due to these missing galaxies, we have redone the age and metallicity gradient plots for the subsamples of galaxies having $z_{\rm spec} > 0.02$ and $z_{\rm spec} > 0.03$, in order to avoid the regions with higher incompleteness. The trends found for the two subsamples are almost identical to the ones for the full data set, which suggests that the impact on our results of all sources of incompleteness is negligible, both at low and high masses.

It has been suggested that the Sérsic fitting procedure adopted in B05 contain significant biases. In particular, at very high luminosities, Sérsic indices, effective radii and fluxes can be underestimated by ~ 0.5, ~ 10–15 per cent and ~ 10 per cent, respectively (B05). Similar considerations hold for systems with high effective radii and Sérsic indices. The Sérsic procedure used in B05 has been extensively analysed in Guo et al. (2009), who have shown that the main source of systematics is introduced by the 1D Sérsic fit and background sky level estimate. However, these systematics turn out to produce shallower CGs (of ~ 0.03) than our estimates, thus leaving the main trends with luminosity and mass unaffected. On the other hand, for the systems with very low Sérsic indices, the B05 fitting procedure recovers quite well the parameters, although a slight underestimate of fluxes and an overestimate of n might still occur (Guo et al. 2009).

A2 Morphological separation and contamination

Seeking for a trustful morphological classification, the eyeball check and the bulge-to-total mass ratio (B/T) are the best approaches, but unfortunately they are not suitable procedure for very large sample of galaxies (Allen et al. 2006; Lintott et al. 2008). Indeed, the use of some objective automated morphological classification is more efficient. For these reasons, we decided to adopt a classification with the minimal parameter set to minimize the probability of erroneously discarding ETGs, even if this would make the LTG contamination non-negligible. We have 'a posteriori' checked the effect of such a
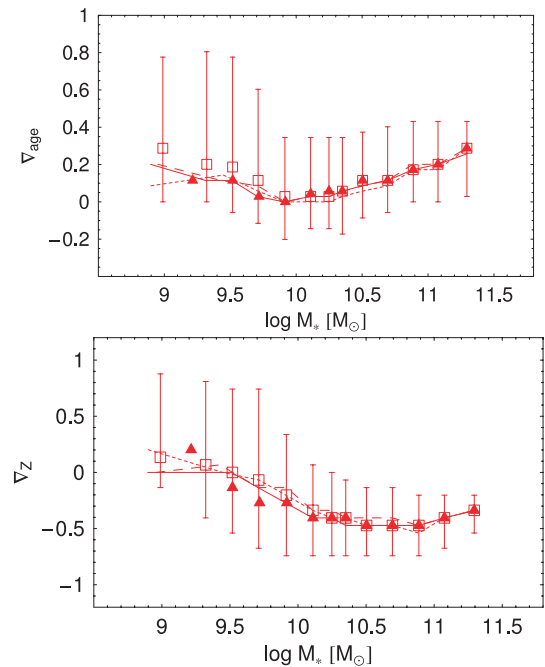

Figure A2. Systematics in the $\nabla_{\rm age}$ and ∇_Z as a function of stellar mass due to changes in selection criteria. Boxes and bars are for our reference results. Continue, long-dashed and short-dashed lines are for (a) $C > 2.6$, (b) $C > 3$ and (c) $2.5 < n < 5.5$, respectively, and triangles for our reference criteria with a cut in the total colour ($g-r > 0.55$).

contamination on the results. We have verified that the use of the *concentration* and Sérsic index n parameters is efficient to this purpose. In fact, the Sérsic index is a measure of the steepness of the surface brightness profile and is historically considered as a good indicator of galaxy type: LTGs are well fitted by light profiles with lower n, being $n = 1$ the prototype of light profile for galaxy discs, and $n > 1$ the ones typical of ETGs. Recently, the concentration parameter determined from the SDSS pipeline has been claimed to be an even better proxy of galaxy morphology (Shimasaku et al. 2001; Strateva et al. 2001; Nakamura et al. 2003; Weinmann et al. 2009). We have checked that the results on the gradient trends do not strongly depend on the constraints adopted on the two parameters for the ETG/LTG separation (see Fig. A2) with some significant change raising for age gradients at $M_* \lesssim 10^{9.5}\,{\rm M_\odot}$. We also analysed the impact on our results when a cut in colour is applied.
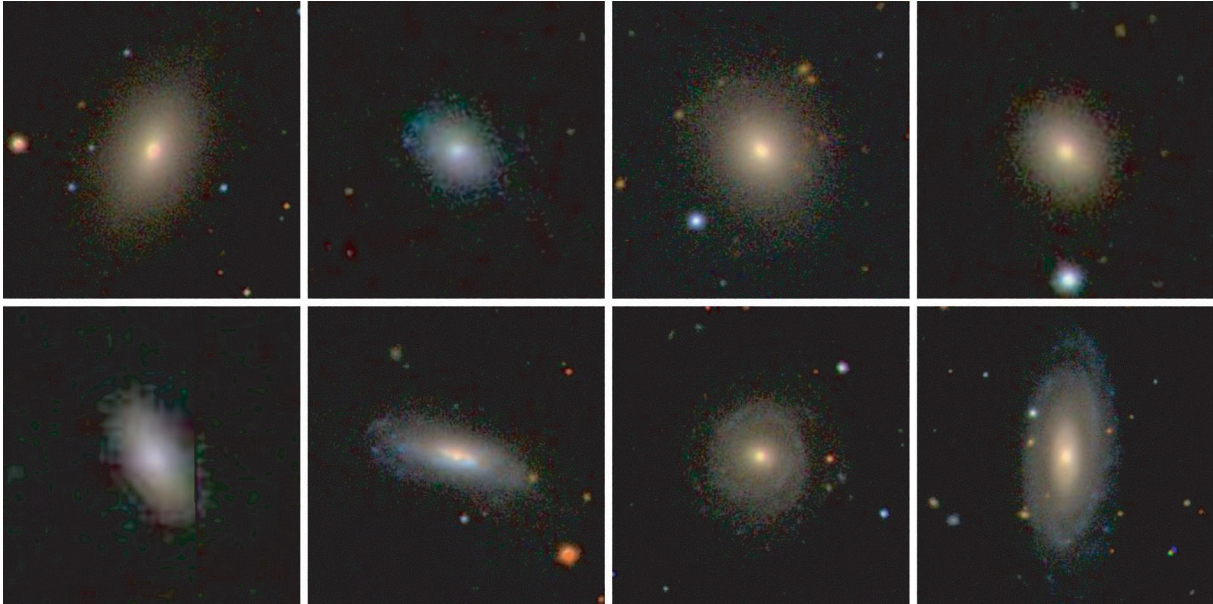
Figure A3. Images of eight galaxies classified by eyeball checking. The galaxies in the top panels are classified as E/S0, the first one in the bottom panels is uncertain, while the last three are clear example of spirals.
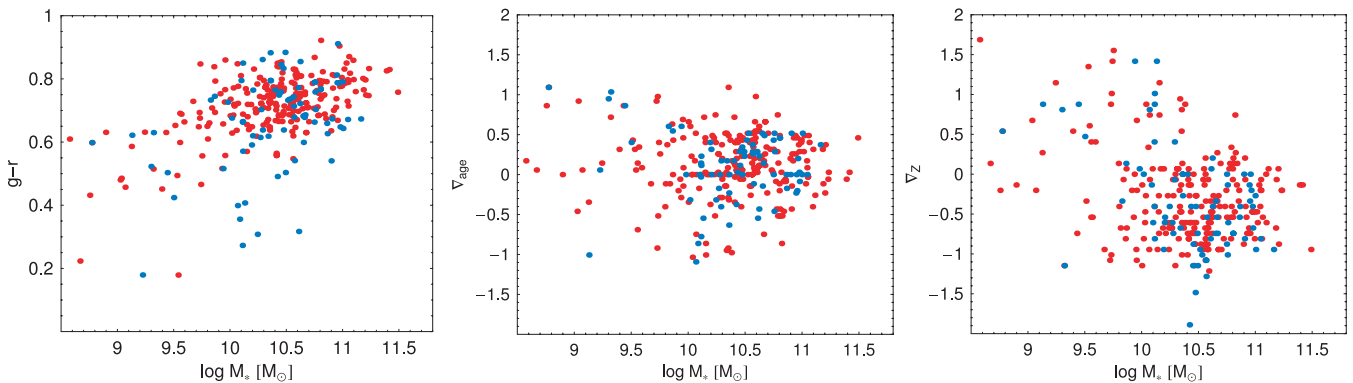

Figure A4. Results for galaxies extracted for eyeball check. The red points are for galaxies classified as ellipticals, while blue ones are for the galaxies with an uncertain classification or spirals. Left-hand panel: colour–mass diagram. Middle panel: $\nabla_{\rm age}$ as a function of stellar mass. Right-hand panel: ∇_Z as a function of stellar mass.

As anticipated, our selection criteria are not meant to be contamination free, with ETGs being possibly contaminated by disc galaxies, e.g. both n and C depend on the inclination and edge-on disc or spiral galaxies can show parameter values typical of ETGs. An approach to avoid this kind of contamination can rely on the axial ratio, but in this case we would loose edge-on S0s misclassified as LTGs (Maller et al. 2009; Weinmann et al. 2009). In order to evaluate the fraction of contaminants in our ETG sample, we have made an eyeball inspection of a subsample of 300 randomly selected galaxies. This classification may be still prone to subjectivity, thus four of us have checked the galaxies and produced an average classification. Eight galaxy images are shown in Fig. A3. We find that ~70–75 per cent of galaxies are ETGs, while the remaining galaxies are uncertain objects or clear spirals. These uncertain or misclassified galaxies mainly fill the intermediate-mass region and many of them have red colours $g - i \gtrsim 0.5$. Although the fraction of such contaminants is not negligible, we have found that the gradients are not strongly biased on average, as shown in Fig. A4. The bottom line of this check is that the inclusion of contaminants leaves the average gradients unaffected. For instance, on the mass range

$10 < \log M_* < 11$, we obtain as median value $\nabla_{\rm age} = 0.12$, and 0.03 for the ETGs and the contaminants, respectively, as shown in Fig. A4, while we find $\nabla_Z = -0.47$ and -0.54 for the same systems. However, when computing the median values for the whole sample, the result is unchanged from the one of systems correctly classified as ETGs. No net difference in the central galaxy age is found, while central metallicity for contaminants is larger than the one for ETGs, consistently with the steeper metallicity gradients for galaxies with larger metallicity (see Fig. 6). We have also checked that the presence of contaminants in ETG sample, in particular, does not affect the dependence on the central age of $\nabla_{\rm age}$ and ∇_Z as discussed in Fig. 4. Thus, we can safely assume that the central age is a genuine parameter which rules the scatter of the relations with mass and σ_0.

Finally, the conservative choice of both n and C provided a quite sharp separation between ETGs and LTGs. For sake of completeness, the residual galaxy sample with a mixed morphology, i.e. ITGs, turned out to have also an intermediate distribution of the age gradients as shown in Fig. A5. On the contrary, metallicity gradients of ITGs have a trend which is more similar to the one of ETGs.
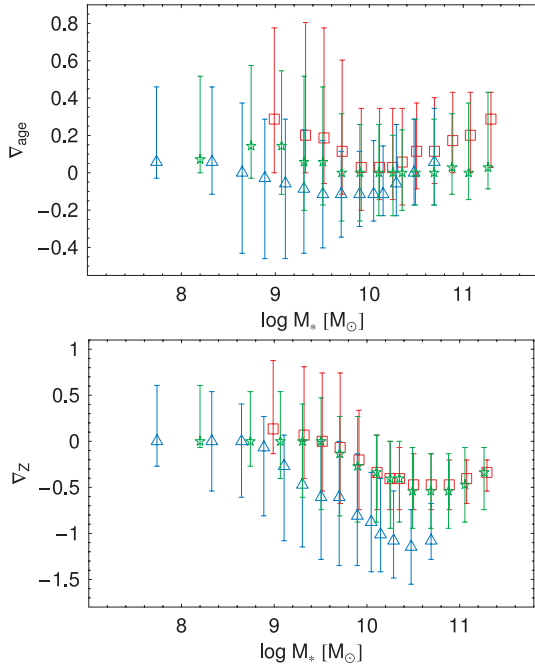
Figure A5. Age (upper panel) and metallicity (lower panel) gradients as a function of stellar mass for ETGs (open red boxes), LTGs (open blue triangles) and ITGs (green open stars).

APPENDIX B: SYSTEMATICS IN STELLAR FITTING

We examine the role of systematic uncertainties on the stellar population results. First, we address the problem of degeneracy in synthetic spectral models (Section B1), then derive the optical-IR and IR CGs from our fitted stellar populations and check the consistency with results from literature (Section B2). Dust extinction is discussed in Section B3.

B1 Parameter degeneracies and wavelength coverage

We have analysed the optical CGs, fitting the internal and external colours with synthetic spectral models to derive the age and metallicity of stellar populations. Because of the well-known age–metallicity degeneracy (Worthey 1994; BC03; Gallazzi et al. 2005), the stellar parameters and the relative gradients might be severely biased, in particular by using the optical colours only. Increasing the wavelength coverage or adding spectral information would be the best approach to the problem.

NIR bands are primarily sensitive to the red stellar populations which represent the main fraction of stars forming an evolved galaxy, allowing to trace the visible mass of old galaxies, and are less affected by dust extinction. Their inclusion is suitable to alleviate the age–metallicity degeneracy (de Jong 1996; Cardiel et al. 2003; MacArthur et al. 2004; Chang et al. 2006), but is not expected to be definitive. Different colours are found to have a different sensitivity to age and metallicity (Li, Han & Zhang 2007). For instance, both optical and IR colours are found to be sensitive to metallicity, while age mostly affects the optical colours (Chang et al. 2006). Wu et al. (2005) showed that the inclusion of NIR bands allows one to recover much more accurate stellar parameters from the fit, but the confidence contours are still affected by the age–metallicity relation, and the gain with respect the optical bands is minimal. It is reasonable to argue that the use of a large statistical sample, as

Table B1. Results from Monte Carlo simulations. We show the median relative age $\Delta(\text{age}) = (\text{age}_{\text{fit}} - \text{age}_{\text{in}})/\text{age}_{\text{in}}$ and metallicity $\Delta(Z) = (Z_{\text{fit}} - Z_{\text{in}})/Z_{\text{in}}$, where *fit* and *in* are for estimated and input parameters. The results for different initial perturbations δ and without or with IR photometry are shown.

		ugriz	*ugrizJHKs*
$\Delta(\text{age})$	$\delta = 0.01$	$0.01^{+0.12}_{-0.10}$	$0^{+0.08}_{-0.07}$
	$\delta = 0.03$	$0.02^{+0.27}_{-0.20}$	$0^{+0.12}_{-0.14}$
	$\delta = 0.05$	$0.03^{+0.49}_{-0.26}$	$0^{+0.25}_{-0.17}$
$\Delta(Z)$	$\delta = 0.01$	$-0.01^{+0.13}_{-0.13}$	$0^{+0.07}_{-0.08}$
	$\delta = 0.03$	$0^{+0.28}_{-0.27}$	$0^{+0.13}_{-0.12}$
	$\delta = 0.05$	$-0.02^{+0.39}_{-0.40}$	$0^{+0.19}_{-0.20}$

we adopt in this paper, is more effective in reducing the overall uncertainties of the galaxy properties than the adoption of a larger filter baseline.

Of course, the adoption of spectroscopic line absorption indices would be the best indicators of stellar population parameters and gradients, as they permit to break the age–metallicity degeneracy (e.g. Burstein et al. 1984; Carollo, Danziger & Buson 1993; Davies et al. 1993; Henry & Worthey 1999; Mehlert et al. 2003). However, spectral indices of large galaxy sample are still difficult to obtain for the observational limits imposed by the low starlight fluxes (e.g. around R_{eff} and beyond). Recently, integral-field spectroscopy has been used to determine gradients in line absorption indices (e.g. Kuntschner et al. 2006; Rawle et al. 2010) of elliptical and lenticular galaxies, but this approach is only applicable to limited samples of systems.

Despite the limited wavelength coverage, but taking advantage of the large statistical sample, we have shown that both spectroscopy and photometric analysis converge to similar results for stellar population gradients (see e.g. Section 3.4). Similarly, Rawle et al. (2010) have shown that optical colours and CGs derived from spectroscopic age and metallicity are generally consistent with values directly recovered from photometry. Moreover, the recovered correlations between metallicity and age gradients are not spurious and not generated by correlated measurement errors on these quantities.

However, in the attempt of putting our result further on a more solid ground, we have tested the reliability of our colour modelling technique and checked for the presence of spuriously generated correlations between age and Z or gradients ∇_{age} and ∇_Z, running several Monte Carlo simulations. We extracted 1000 simulated galaxy spectra from our BC03 spectral energy distribution libraries with random (age$_i$, Z_i) for $i = 1, 2$ (i.e. with no correlations among these parameters and with ∇_Z, and ∇_{age} randomly distributed), and applied our fitting procedure, comparing the estimated parameters with the input model values. We perform the fit (1) only using the optical SDSS bands *ugriz* and (2) adding the *JHKs* photometry from 2MASS survey (Jarrett et al. 2003), to understand the systematics that the fit of optical colours can induce. Typical observational uncertainties for each band are assigned (i.e. $\delta u \sim 0.06$, $\delta g \sim 0.035$, $\delta r \sim 0.035$, $\delta i \sim 0.035$, $\delta g \sim 0.04$, $\delta J \sim 0.08$, $\delta H \sim 0.12$, $\delta Ks \sim 0.09$, from matched catalogue in B05) and the input model colours are perturbed adding a random step in the interval $(-\delta, +\delta)$ with $\delta = 0.01, 0.03, 0.05$ to account for measurement systematics. Results of this analysis are collected in Table B1 and Fig. B1. We found that, on average, both the stellar parameters and gradients are fairly well recovered from the fitting procedure, with a scatter increasing with δ, and no
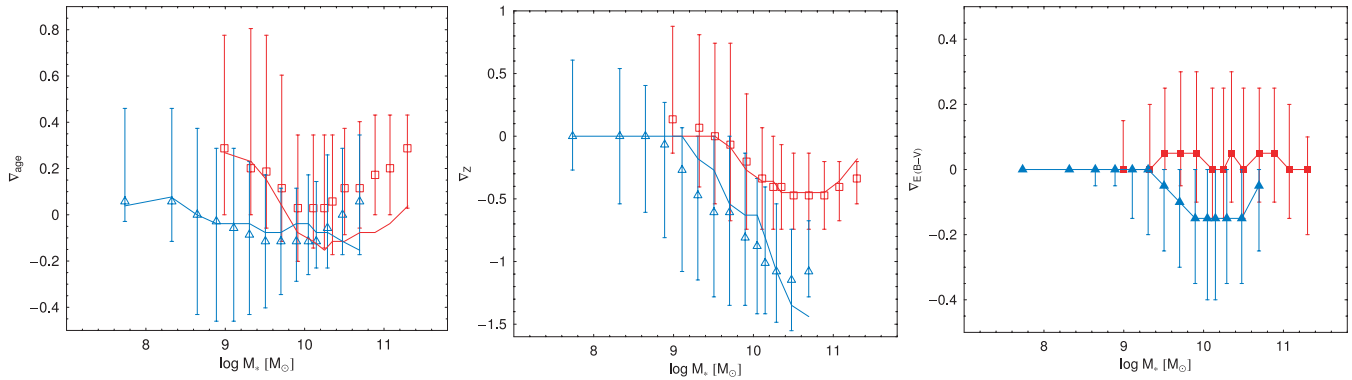
Figure B2. Gradients for the spectral model leaving free the galaxy age, metallicity and dust content. The open symbols with bars are for our reference fit, while the line is for the fit with dust extinction free to vary. Left-hand panel: ∇_{age} as a function of stellar mass. Middle panel: ∇_Z as a function of stellar mass. Right-hand panel: gradient in dust extinction as a function of stellar mass.
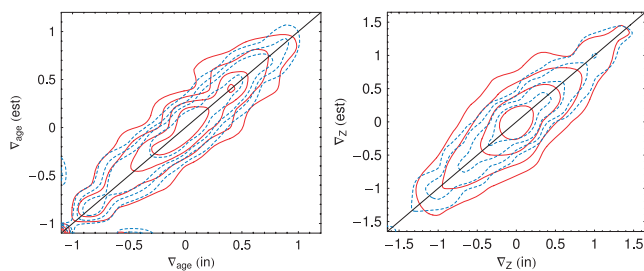

Figure B1. Comparison of age (left) and metallicity (right) gradients estimated from Monte Carlo repetitions (y-axis), given the initial input values (x-axis). Here we consider our extreme error budget, $\delta = 0.05$. Red and dashed blue contours are the isodensity corresponding to the results from the stellar population fit, using only optical and optical+IR colours, respectively.

spurious correlations are induced at more than 99 per cent confidence level (see also Wu et al. 2005 and Tortora et al. 2009a, for similar analysis). We confirm the finding of Wu et al. (2005) that the inclusion of NIR bands allows a better recovery of the input stellar parameters with a scatter in the range 5–25 per cent, while the scatter is larger (in the range 10–50 per cent) when only SDSS bands are used. Thus, the most remarkable result of this analysis is that, notwithstanding the larger scatter, we are able to successfully recover the stellar population parameters, even without NIR photometry.

B2 Comparison with IR CGs

One of the advantages of synthetic spectral modelling is to allow the recover of synthetic IR colours by using the best-fitted spectral parameters. Therefore, we derive the colours $g-J$, $g-H$ and $g-Ks$ at $0.1R_{eff}$ and $1R_{eff}$ and the relative CGs, which show trends with mass similar to those discussed in this paper. If we select luminous ($r < -20$ mag) ETGs, we find median values of $\nabla_{g-J} = -0.33$, $\nabla_{g-H} = -0.37$ and $\nabla_{g-Ks} = -0.40$, with 25–75 percentiles in sample distribution of 0.17, 0.18 and 0.20, respectively. As already extensively discussed in the text, to compare these synthetic CGs with the observed values in La Barbera & de Carvalho (2009), we select older systems with $age_1 > 6$ Gyr. In this case, we have $\nabla_{g-J} = -0.26$, $\nabla_{g-H} = -0.29$ and $\nabla_{g-Ks} = -0.31$ (with scatter of 0.16, 0.18, and 0.20), which are fairly consistent with the results reported by these authors. A fairly good agreement is also found with the median $\nabla_{g-Ks} = -0.29 \pm 0.07$ in Wu et al. (2005).

B3 Internal dust extinction

In our analysis we have assumed no internal extinction. This assumption is more reasonable for ETGs, where only a negligible fraction of interstellar matter is in the form of dust (e.g. Kormendy & Djorgovski 1989; Wise & Silva 1996; Dorman, O'Connell & Rood 2003), but it might be inappropriate for LTGs, as these systems have a larger amount of internal dust (e.g. Brammer et al. 2009). Usually no dust extinction is included in the analysis of ETGs (Tamura & Ohta 2000; Tamura et al. 2000; Tamura & Ohta 2003; Wu et al. 2005), but dust gradients would have effects in CGs (e.g. Goudfrooij & de Jong 1995). However, for ETGs it has been shown that metal absorption lines gradients, being less affected by dust extinction than colours (e.g. MacArthur 2005), are unlikely to be produced by pure dust extinction gradients to mimic the population gradients inferred by broad-band colours (Peletier et al. 1990a; Carollo et al. 1993; Davies et al. 1993; Kobayashi & Arimoto 1999; Rawle et al. 2010). Thus they are not dominant but could still contribute to a fraction of CGs. Similarly, in LTGs the dust seems to have a negligible effect in shaping CGs (e.g. MacArthur et al. 2004), even though there are still open questions (MacArthur et al. 2009) which might lead to a different conclusion. To analyse the impact of dust extinction on our results, we fit the colours at $0.1R_{eff}$ and $1R_{eff}$ using a library of spectra with age, metallicity and dust content free to change. The extinction curve of Cardelli, Clayton & Mathis (1989) is used to account for the extinction contribution in different wavebands and the colour excess $E(B-V)$ in the range 0–0.5 is used as a free parameter. The results are shown in Fig. B2, where they are compared with our reference results with no dust. The main trends are unaffected by the dust, although we note some differences in the ∇_{age} at $M_* \gtrsim 10^{9.5}$ M$_\odot$. On the other hand, only slight differences are observed for metallicity gradients, and the qualitative trends are unaffected both in ETGs and LTGs. Thus this analysis has shown that, although dust extinction is not negligible in both ETGs and LTGs, the trends and the amplitude of gradients are still dominated by changes in stellar population parameters. We show the dust extinction gradients, defined as $\nabla_{E(B-V)} = E(B-V)_2 - E(B-V)_1$ in the right-hand panel of Fig. B2. On average, the ETGs exhibit null or slightly positive dust gradients (with a tail towards negative values too), while LTGs have opposite behaviour with a larger dust content in the inner regions, showing steeper dust gradients at intermediate high masses (e.g. Dalcanton & Bernstein 2002; MacArthur et al. 2004). Finally, we have checked the absence of any correlation between age and metallicity gradient with both $\nabla_{E(B-V)}$ and the central extinction for LTGs which has suggested that the results of

these systems are not affected by the presence of dust. We remark that the use of only optical bands and the addition of IR photometry is not sufficient to break the degeneracy between stellar population parameters and dust, for this reason we are tempted to consider these results more as a caveat for this particular data set rather than a conclusive check. If the correction of the age gradients for the dust extinction is right, the net effect is that the age gradient might be less affecting the CG for massive systems and only metallicity gradient should matter.

This paper has been typeset from a TEX/LATEX file prepared by the author.